THE JOURNAL OF PHYSICAL CHEMISTRY C

Article

Cite This: J. Phys. Chem. C 2018, 122, 27893−27916

pubs.acs.org/JPCC

1,7-Dipyrene-Containing Aza-BODIPYs: Are Pyrene Groups Effective as Ligands To Promote and Direct Complex Formation with Common Nanocarbon Materials?

Yuriy V. Zatsikha,[†] Tanner S. Blesener,[†] Philip C. Goff,[‡] Andrew T. Healy,[‡] Rachel K. Swedin,[‡] David E. Herbert,[†] Gregory T. Rohde,[§] Kullapa Chanawanno,[∥] Christopher J. Ziegler,[⊥] Rodion V. Belosludov,[*,#] David A. Blank,[*,‡] and Victor N. Nemykin[*,†]

[†]Department of Chemistry, University of Manitoba, Winnipeg, Manitoba R3T 2N2, Canada

[‡]Department of Chemistry, University of Minnesota, Minneapolis, Minnesota 55455, United States

[§]Marshall School, Duluth, Minnesota 55811, United States

[∥]Department of Chemistry, Faculty of Science, Chiang Mai University, Chiang Mai 50200, Thailand

[⊥]Department of Chemistry, University of Akron, Akron, Ohio 44325, United States

[#]Institute for Materials Research, Tohoku University, Sendai 980-8577, Japan

Supporting Information

ABSTRACT: A series of 1,7-dipyrene-aza-BODIPY and 1,7-dipyrene-3,5-diferrocene-aza-BODIPY derivatives **5a−e** with pyrene ligands covalently attached to the *β*-pyrrolic positions of the boron-azadipyrromethene (aza-BODIPY) core have been prepared and characterized by NMR, UV−vis, and steady-state fluorescence spectroscopy; high-resolution mass spectrometry; and X-ray crystallography. The redox processes of these donor−acceptor aza-BODIPY systems were investigated by electrochemistry (cyclic voltammetry and differential pulse voltammetry methods) and spectroelectrochemistry. The potential of the closely spaced 1,7-dipyrene fragments to promote formation of noncovalent *π*-complexes with nanocarbon materials (C_{60}, C_{70}, (6,5)-single-walled carbon nanotube, and graphene) was explored. UV−vis, steady-state fluorescent, and time-resolved transient absorption spectroscopy data indicated that the interaction between the new pyrene-aza-BODIPYs and C_{60} or C_{70} fullerenes in solution is weak, and time-resolved transient absorption spectroscopy provided no evidence of photoinduced electron transfer. X-ray crystallography on a binary solid of aza-BODIPYs **5b** and C_{60} was indicative of a pyrene−pyrene rather than pyrene−C_{60} interaction motif, whereas fullerenes were found to form close contacts with the electron-rich B,O-chelated part of aza-BODIPY **5b**. In contrast, pyrene−pyrene and pyrene−C_{60} but not aza-BODIPY−C_{60} interactions were observed in the crystal structure of aza-BODIPY **5d** and C_{60}. Density functional theory (DFT) and time-dependent DFT calculations were used to support conclusions based on experimental data and are suggestive of rather weak interaction energies between 1,7-dipyrene-aza-BODIPYs and nanocarbon materials. Direct comparison with an analogous control compound lacking the pyrene ligands demonstrated that the pyrene substituents were ineffective at promoting and directing complex formation with nanocarbon materials. A common measurement of complex formation, emission loss in the presence of a nanocarbon acceptor, was demonstrated to have an alternative explanation in these systems, and the general effectiveness of using pyrene ligands to build noncovalent complexes was drawn into question.

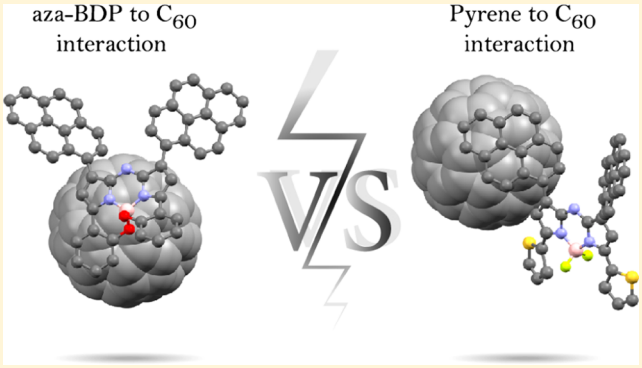

INTRODUCTION

Facile formation of stable, long-lived, and charge-separated states is an important initial step in the preparation of efficient organic solar cells.[1−5] There are many examples of covalently bound donor−acceptor (D−A) systems, where strong binding provides stability and some degree of design control over the electronic coupling.[6−19] When substituted with electron-donating groups capable of intramolecular electron transfer, porphyrins,[20−31] phthalocyanines,[32−40] subphthalocyanines,[41−47] boron-dipyrromethenes (BODIPYs),[48−54] and boron-azadipyrromethenes (aza-BODIPYs)[55−60] have been demonstrated to be effective and stable assemblies for initial light absorption and charge separation. Organic amines[61−72] and ferrocene,[73−88] as examples, have been shown to be

Received: September 28, 2018
Revised: November 6, 2018
Published: November 14, 2018

DOI: 10.1021/acs.jpcc.8b09504
J. Phys. Chem. C 2018, 122, 27893−27916

Scheme 1. Synthetic Pathway for Preparation of Aza-BODIPYs 5a−e

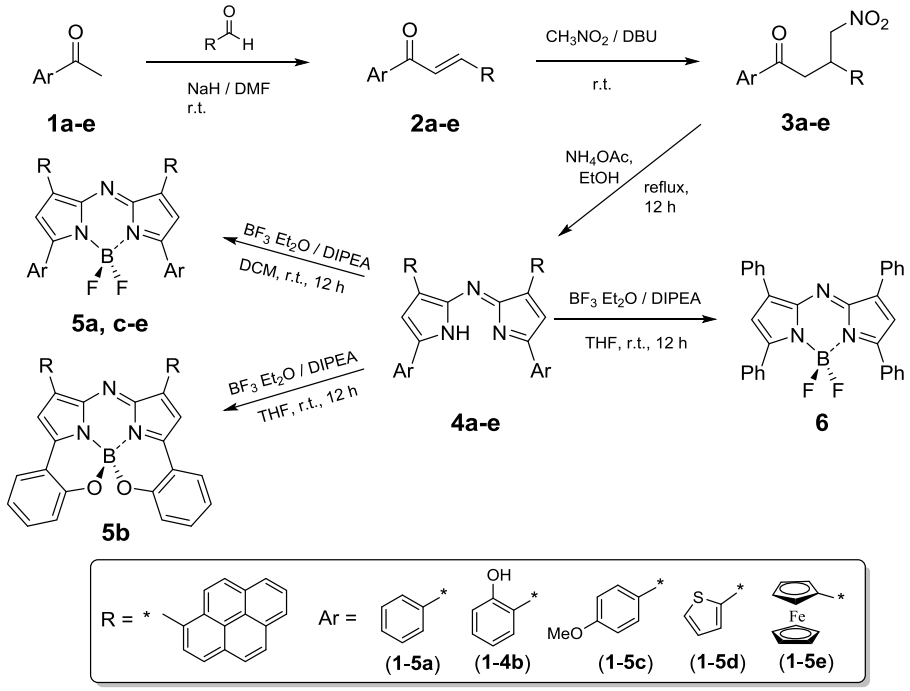

effective electron-donating groups capable of facilitating photoinduced intramolecular electron transfer. Formation of noncovalent D−A systems has received considerable attention in recent years.[1−5,89−101] While the potential advantages of noncovalent systems include self-assembly upon simple mixing, the weaker bonding in noncovalent D−A systems can compromise stability and increase conformational disorder. It becomes challenging to control the relative D−A geometry and orientation, which is the key to tuning the degree of electronic coupling between the donor and acceptor.[102−111] There are examples demonstrating efficient formation of long-lived photoinitiated charge-transfer states between conjugated chromophore donors and noncovalently associated fullerenes, carbon nanotubes, and graphene.[112−121] Formation and stability of these noncovalent D−A assemblies rely on enhancement of dispersion forces and electronic coupling provided by $\pi-\pi$ interactions and topologies that facilitate strong spatial overlap.

The pyrene ligands installed have been reported to serve as effective noncovalent linkers to nanocarbon surfaces,[122−128] and evidence for photoinduced electron transfer between organic chromophores and a nanocarbon surface following excitation at around 400 nm has been presented. We report the synthesis and characterization of a series of 1,7-dipyrene aza-BODIPYs (**5a−e**, Scheme 1 and Synthesis and Characterization of 5a−e) and the subsequent investigation of noncovalent complex formation with potential nanocarbon electron acceptors in solution (Titration with Nanocarbon Materials in Solution) and in the solid state (Solid-State Mixtures). Two covalently linked pyrene groups at the β-positions of the aza-BODIPYs were hypothesized to facilitate noncovalent interactions with nanocarbon materials such as C_{60} and C_{70} fullerenes, (6,5)-single-walled carbon nanotube (SWCNT), and graphene. Some of the experimental observations are consistent with results in analogous studies that were presented as strong support for the presence of excited-state charge transfer and the hypothesis that pyrene ligands mediated complexation of other chromophores with nanocarbon partners.[1−5,124] However, we demonstrate that the observations presented here are not the result of charge transfer and do not provide evidence of strong pyrene-mediated association.

RESULTS AND DISCUSSION

Synthesis and Characterization of 5a−e. We have used a typical chalcone-based synthetic strategy[129−131] for the preparation of pyrene-containing aza-BODIPYs **5a−e** and the reference 1,3,5,7-tetraphenyl-aza-BODIPY **6** (Scheme 1). A variety of aryl substituents located at the α-positions were chosen to modulate electron density at the aza-BODIPY core. Chalcones **2a−e** were synthesized by the condensation reaction of 1-pyrenecarboxaldehyde and the corresponding ketones **1a−e** with subsequent nitromethylation to form products **3a−e**. Nitromethyl derivatives **3a−e** were converted to the corresponding azadipyrromethenes **4a−e** by reaction with ammonium acetate and then to the final pyrene-containing aza-BODIPYs **5a−e** by reaction with boron trifluoride solution. All new compounds were characterized by ^{1}H and ^{13}C NMR spectroscopy, high-resolution mass spectrometry (HRMS), and UV−vis spectroscopy (Experimental Procedure and Figures S1−S33, Supporting Information). The NMR spectra of all target compounds confirm their symmetric nature, while high-resolution mass spectra are in full agreement with their elemental composition.

The molecular structures of **4e**, **5a**, **5d**, and **5e** were confirmed by X-ray crystallography (Figure 1). Relatively large torsional angles between the two phenyl substituents and the aza-BODIPY core in **5a**, ∼35.84 and ∼43.10°, inhibited conjugation between the substituents and the chromophore's π-system. The torsional angles were much smaller in **5d** and **5e**. The crystal structure of **5d** had torsion angles between the thiophene group and aza-BODIPY core that varied between ∼0.90 and ∼29.94°, and in **5e**, the torsion angles between the ferrocene group and aza-BODIPY core varied between 6.64

DOI: 10.1021/acs.jpcc.8b09504
J. Phys. Chem. C 2018, 122, 27893−27916

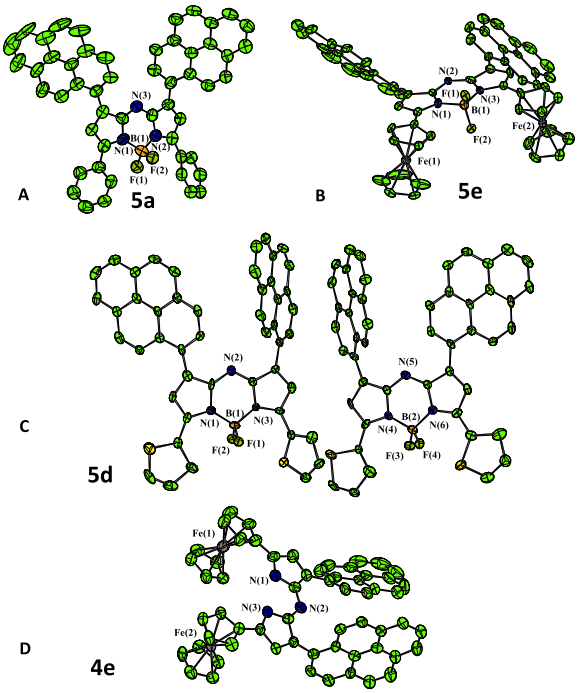

Figure 1. CAMERON representation of BODIPYs **5a** (A) and **5e** (B), two crystallographically independent molecules of **5d** (C), and aza-DIPY **4e** (D), with thermal ellipsoids shown at 50% probability level. All hydrogen atoms are omitted for clarity.

and 17.10°. The observation of a nearly coplanar arrangement between the aza-BODIPY core and the ferrocene substituents in **5e** and the relatively short Fe−Fe distance (~8.13 Å) should facilitate electron transfer between the ferrocene donor and the aza-BODIPY acceptor, as previously observed in the phenyl analogue of **5e**.[132]

In the crystal structures of **4e**, **5a**, **5d**, and **5e**, both pyrene groups are rotated away from the aza-BODIPY π-system (the torsion angles vary between ~33.82 and ~44.78° for **5a**, ~36.64 and ~53.68° for **5d**, and ~48.04 and ~51.62° for **5e**), which reflects the steric bulk of pyrene. Interestingly, the pyrene fragments in **5a** do not form the typical intermolecular $\pi-\pi$ stacking motif. Rather, they form close slipped-stack-type contacts with both the aza-BODIPY core and the pyrene group from a neighboring molecule of **5a**. The closest pyrene−pyrene intermolecular contact observed in the crystal structure of **5a** is ~3.35 Å, which is close to the pyrene-β-pyrrolic (~3.34 Å) and pyrene-α-pyrrolic (~3.32 Å) intermolecular contacts. In the ferrocene-containing **5e**, both slipped-stack (~3.19 to ~3.26 Å) and H-type (~3.35 to ~3.36 Å) close pyrene−pyrene contacts were observed in the crystal structure. With the thiophene-containing **5d**, only H-type (~3.34 to ~3.39 Å) pyrene−pyrene stacking was observed in the crystal structure. In contrast to that in the X-ray crystal structures of **5d** and **5e**, the aza-BODIPY core in the crystal structure of **5a** adopts an unusual, slightly domed conformation. Doming occurs away from the two bulky pyrene fragments. Important for the potential to form noncovalent complexes with nanocarbon partners, the X-ray crystallography data on **5a**, **5d**, and **5e** suggest a large enough cavity between two pyrene groups to accommodate both fullerene and (6,5)-SWCNT in a chelate-type geometry.

The UV−vis spectra of **5a−e** are presented in Figure 2 and can be separated into three general categories. The first consists of **5b−d**, with UV−vis spectra, typical for this class of compounds (for instance reference compound **6**), dominated by a single narrow band in the visible range followed by several lower-intensity components.[129−131] The key differences between UV−vis spectra of **5b−e** and **6**, which lack the pyrene ligands, are the broader low-intensity bands in the visible range and the presence of intense and characteristic absorption bands at ~275 and ~345 nm that are associated

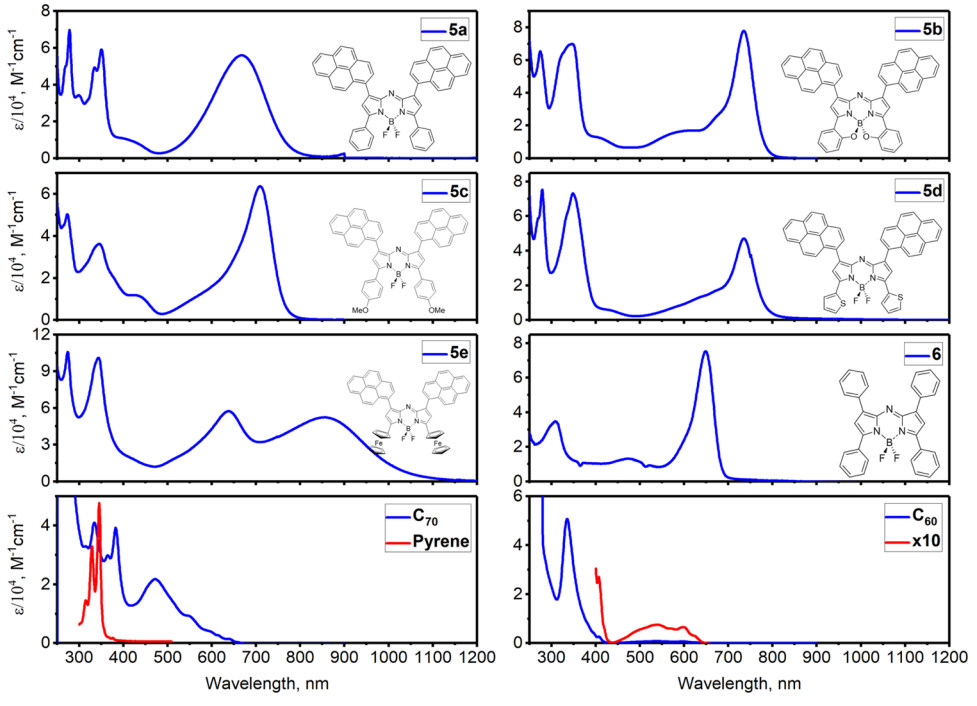

Figure 2. UV−vis spectra of aza-BODIPYs **5a−e** and **6** as well as reference compounds in dichloromethane (DCM).

DOI: 10.1021/acs.jpcc.8b09504
J. Phys. Chem. C 2018, 122, 27893−27916

with the pyrene constituents in **5b–e** (Figure 2). The second category is represented by the phenyl derivative **5a** that has a broad and intense single low-energy band in the visible region and narrow bands at wavelengths shorter than 400 nm primarily localized on the pyrene fragments. The last category is represented by the ferrocene derivative **5e**. It has two intense low-energy bands observed at 638 and 856 nm that are in good agreement with a previously reported diphenyl-ferrocene analogue.[132] The low-energy broad band observed at 856 nm was assigned to the metal-to-ligand charge-transfer (MLCT) transitions, and the narrower band observed at 638 nm was assigned to an aza-BODIPY-centered $\pi-\pi^*$ transition. In general, the energy of the most intense $\pi-\pi^*$ transition observed in **5a–d** correlates well with the density functional theory (DFT)-predicted (discussed below) electron-donating ability of the substituents located at the α-positions of the BODIPY core, **5a** < **5c** < **5b** ~ **5d**.

Steady-state fluorescence spectra are shown in Figures 3 and S34. Fluorescence from the ferrocene-containing **5e** was completely quenched, which is typical for ferrocene-containing BODIPYs[133−137] and aza-BODIPYs.[132,138,139] The fluorescence quantum yields for **5a–d** were significantly smaller than those for other BODIPY compounds,[140,141] reflecting the electron-donating role played by the installed pyrene substituents. The fluorescence spectrum of **5a** was an approximate mirror image of its absorption spectrum with a significant Stokes shift of 2570 cm^{-1} (Table 1). Following excitation at 275 and 345 nm, predominantly centered on the pyrene substituents, emission was observed from **5a–d** in the visible and near-IR regions, clearly indicating energy transfer from pyrene substituents to the aza-BODIPY core; see Figure S34. In the case of thiophene-containing compound **5d**, the pyrene-centered fluorescence peak is much stronger than the aza-BODIPY emission peak, whereas the opposite trend was observed for **5a–c** upon excitation at 275 and 345 nm, which is indicative of much better energy transfer from pyrene fragments to the aza-BODIPY core in compounds **5a–c** (Figure S34). Although one might speculate that the anomalous behavior of the thiophene-containing **5d** can be attributed to the presence of the heavier sulfur atoms in this compound, at this moment, we do not have a clear explanation for such experimental observation.

Excited-state lifetimes are reported in Table 1. At 1–2 ns, the lifetimes for **5a–d** are all similar to reported values for analogous BODIPYs and aza-BODIPYs systems.[140] The data and fits are presented in Figures S35–S38. The data were well-fitted with a single exponential decay. No longer-lived emission was found within the signal-to-noise ratio in the experiments, leaving no evidence for the formation of a triplet state. This is in contrast with the reports of triplet state formation following excitation of *meso*-pyrene BODIPYs.[142,143]

Time-resolved pump–probe transients for the nonfluorescent ferrocene-containing **5e** are shown in Figure 4. The decay of the transient absorption feature centered at 475 nm was well-fitted with a single exponential having a time constant of 1.7 ns (Table 1). This is consistent with the excited-state lifetimes of **5a–d**, and we assign this state to a π^* excited state involving both the aza-BODIPY core and the pyrenes. It is interesting to note that the lifetime of this state is substantially longer than the 176 ps lifetime of the excited state we previously reported for the analogous BODIPY diphenyl diferrocene system.[144,145] In that system, we assigned the

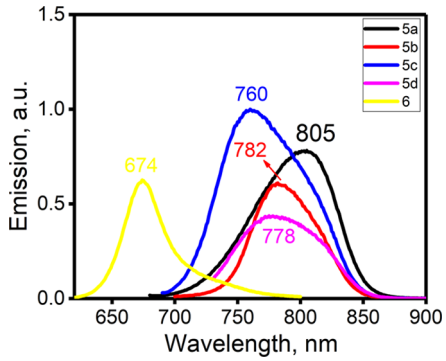

Figure 3. Fluorescence spectra of the aza-BODIPYs **5a–d** and **6** in DCM. Excitation wavelengths are as follows: 650 nm (**5a**), 680 nm (**5b**), 670 nm (**5c**), 700 nm (**5d**), and 600 nm (**6**).

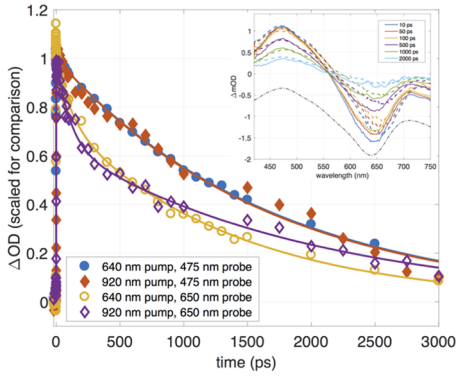

Figure 4. Pump–probe response for **5e**. Symbols are the data, and lines are fits as described in the text. Data probed at 650 nm has been inverted for comparison with data probed at 475 nm. Inset: transient full-frequency spectra at indicated pump–probe delay times. The solid lines represent the data pumped at 640 nm, and the dashed lines represent the data pumped at 920 nm. The dash-dotted line represents the absorption spectrum inverted as a guide to the shape of the bleach component in the pump–probe spectra.

Table 1. Selected Photophysical Properties of 5a–e and the Reference Compound 6[a]

compound	λ_{abs} [nm] (ε [M^{-1} cm^{-1}])	emission [nm] (Φ)	τ [ns]
5a	335 (49 000), 351 (59 000), 667 (55 000)	805 (0.006)	0.87 ± 0.07
5b	347 (70 000), 735 (78 000)	436, 782 (0.0076)	1.6 ± 0.1
5c	346 (36 000), 709 (64 000)	398, 760 (0.0167)	1.1 ± 0.1
5d	347 (73 000), 735 (47 000)	421, 778 (0.0142)	1.3 ± 0.1
5e	344 (101 000), 638 (57 000), 854 (52 000)		1.7 ± 0.2
6	308 (35 000), 648 (75 000)	674 (0.34)	

[a]Lifetimes were determined by transient absorption for all compounds. Data are presented in Figures 4 and S35–S38.

DOI: 10.1021/acs.jpcc.8b09504
J. Phys. Chem. C 2018, 122, 27893–27916

excited-state lifetime to charge recombination following excitation that immediately produced a charge transfer from the ferrocene to the aza-BODIPY core. As shown in Figure 4, unlike the transient absorption at 475 nm that decayed as a single exponential, to obtain a reasonable fit to the recovery of the ground-state bleach probed at 650 nm, a second exponential decay component with a time constant of ca. 100 ps becomes statistically significant in the data (Figure 4). Addition of the faster component is consistent with overlapping transitions in the excitation that includes both the pyrene-centered excitation and ferrocene-to-aza-BODIPY core charge transfer. The shorter time constant is consistent with the time scales for charge recombination that we reported in similar ferrocene-appended BODIPY systems.[144] Increase in the amplitude and subtle change in shape of the transient difference spectra with excitation at 920 nm compared to those at 640 nm are also consistent with the expectation that there should be an increase in the contribution from the charge-transfer transition as the excitation moves to a longer wavelength.

The redox properties of **5a−e** were investigated by electrochemical methods (cyclic voltammetry (CV) and differential pulse voltammetry (DPV)). The data are summarized in Table 2 and shown in Figures 5 and S39. In the cases of **5a−d** and the reference compound **6**, one oxidation and two reduction processes associated with the aza-BODIPY core were observed. Both reduction processes were quasi-reversible, in agreement with the literature data.[144,146,145] The first reduction potentials were all within 100 mV of each other, indicating limited influence of the substituents located at the α-position of the corresponding aza-BODIPY. This is consistent with the significant contribution from the nitrogen atoms to the lowest unoccupied molecular orbital (LUMO) in aza-BODIPY, as discussed below. The first oxidation process is quasi-reversible in **5a−c** and irreversible in **5d**. The larger range of oxidation potentials across the series is consistent with the significant contribution from the α-pyrrolic carbon atoms to the highest occupied molecular orbital (HOMO) in aza-BODIPYs. Irreversible oxidation of the pyrene groups in **5a−d** was observed at higher potentials (Table 2, Figures 5 and S39). A single broad two-electron oxidation wave was observed in the CV and DPV experiments on **5b−d**. With **5a**, two one-electron oxidation waves associated with a stepwise oxidation of the pyrene groups were clearly resolved in the DPV experiments. In the case of the ferrocene-containing **5e**, the first and second reduction processes remained reversible and were attributed to the reduction of the aza-BODIPY core. The first reduction potential is more negative in **5e** than in **5a−d**. The first and second single-electron oxidations were assigned to the stepwise oxidation of two ferrocene groups in **5e**. Both of these oxidations were quasi-reversible, and the difference between them, 460 mV, is similar to that observed for the phenyl analogue of **5e**.[132] More interestingly, three additional single-electron oxidation waves were observed in CV and DPV experiments on **5e**. The first quasi-reversible oxidation in **5e**, Ox_3 in Table 2, was assigned to oxidation of the aza-BODIPY core, whereas the other two, closely spaced at the higher potentials, Ox_4 and Ox_5, were attributed to the stepwise irreversible oxidation of the pyrene fragments.

To characterize spectroscopic signatures of the redox-active species generated upon stepwise oxidation of the ferrocene groups in **5e**, we conducted spectroelectrochemical oxidation experiments (Figure 6). Similar to the phenyl analogue of **5e**,[132] during the first oxidation process, a new broad band appeared in the near-infrared (NIR) region (~1000 nm). In addition, a very broad band between ~1500 and 2600 nm appeared in the spectrum, very characteristic for diferrocene-BODIPY compounds.[132] Simultaneously, the initial bands at 557 and 685 nm were transformed into a single broad band observed at 577 nm. The broad band at ~2500 nm is characteristic of mixed-valence diferrocenyl-[132] and tetraferrocenyl-containing[147] aza-BODIPYs and is indicative of formation of the mixed-valence $[\mathbf{5e}]^+$. Band deconvolution analysis of the NIR region of the UV−vis−NIR spectrum of $[\mathbf{5e}]^+$ is suggestive of the class II (weakly coupled) behavior of this mixed-valence compound (Figure S40).[148−150] During the second oxidation process, the NIR bands are diminished and the final spectrum is dominated by a very characteristic strong aza-BODIPY-centered $\pi-\pi^*$ transition observed at 593 nm. The presence of this band in doubly oxidized $[\mathbf{5e}]^{2+}$ indicates that the aza-BODIPY chromophore is not significantly affected upon stepwise oxidation of **5e**, which is consistent with a stepwise oxidation of the two ferrocene groups.

To correlate experimentally observed spectroscopic and redox properties with the electronic structure, DFT and time-dependent DFT (TDDFT) calculations were performed on **5a−e**. The predicted frontier orbital compositions are shown

Table 2. Redox Properties of 5a−e and the Reference Compound 6[a]

compound	E_{Ox}^4 (V)	E_{Ox}^3 (V)	E_{Ox}^2 (V)	E_{Ox}^1 (V)	E_{Red}^1 (V)	E_{Red}^2 (V)
5a			1.0*	0.7	−0.86	−1.6*
5b			1.0*	0.62	−0.91	−1.5*
5c			1.05*	0.57	−0.91	−1.63*
5d			0.95*	0.57*	−0.81	−1.55*
5e	1.1*	0.85	0.44	0	−1.16	−1.84
6				0.84	−0.85	−1.65
6[60]				0.76	−0.79	−1.54

[a]All potentials are referenced to the FcH/FcH^+ couple in DCM/0.05 M tetrabutylammonium terakis(pentafluorophenyl)borate (TFAB). "*" denotes an irreversible or a partially reversible process.

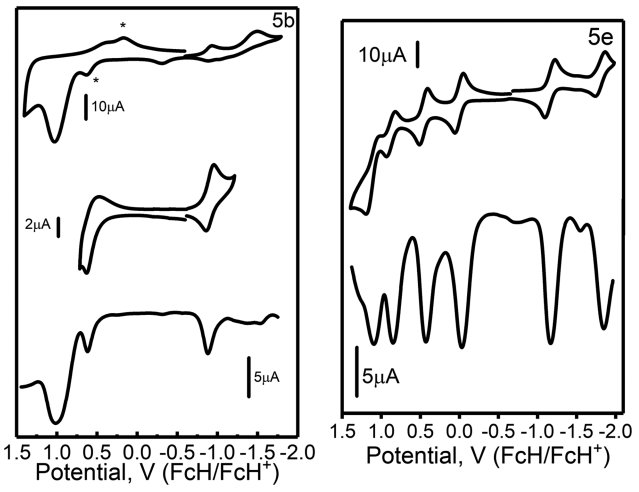

Figure 5. CV and DPV data for aza-BODIPYs **5b** and **5e** in DCM. * Indicates degradation products originated from the irreversible oxidation processes.

DOI: 10.1021/acs.jpcc.8b09504
J. Phys. Chem. C 2018, 122, 27893−27916

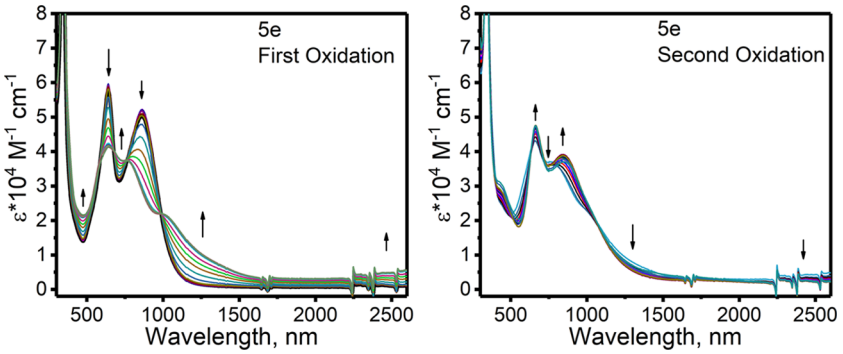

Figure 6. Spectroelectrochemical oxidation of compound **5e** in the DCM/0.15 M TFAB solvent system: the first oxidation process (left) and the second oxidation process (right).

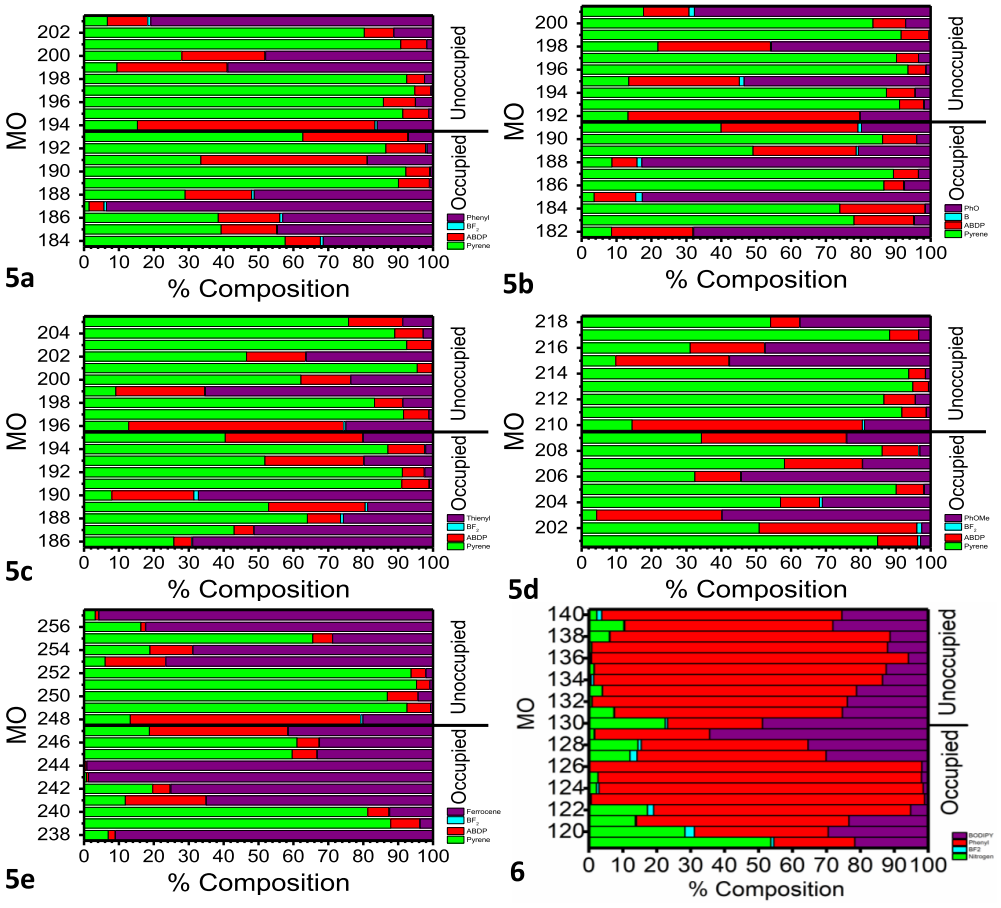

Figure 7. DFT-predicted compositions of frontier orbitals for compounds **5a**−**e** and **6**.

in Figure 7, an energy-level diagram is presented in Figure 8, and the important frontier orbitals are pictured in Figure 9. In the case of reference 1,3,5,7-tetraphenyl-aza-BODIPY **6**, DFT predicts that the HOMO is primarily localized at the α- and β-position of the chromophore's core, which is typical for BODIPYs and aza-BODIPYs.[133−137] In addition to this, **5a**−**d** have significant (~20−50%) contributions from the pyrene fragments, whereas HOMO − 1 and HOMO − 2 were predicted to have dominant pyrene character. DFT predicts that the LUMO in **5a**−**d** is localized on the pyrrolic- and *meso*-nitrogen atoms, which is common for aza-BODIPY chromophores.[133−137] The energy of the HOMO follows the electron-donating ability of the functional group attached at the α-position of aza-BODIPY, as one might expect. A large

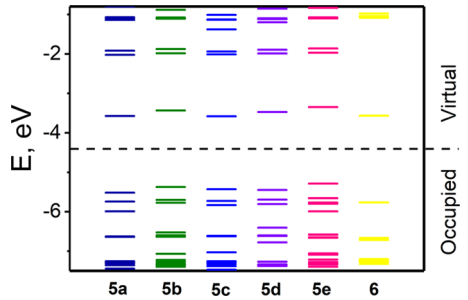

Figure 8. DFT-predicted energy diagram for the frontier MOs in **5a**−**e** and **6**.

DOI: 10.1021/acs.jpcc.8b09504
J. Phys. Chem. C 2018, 122, 27893−27916

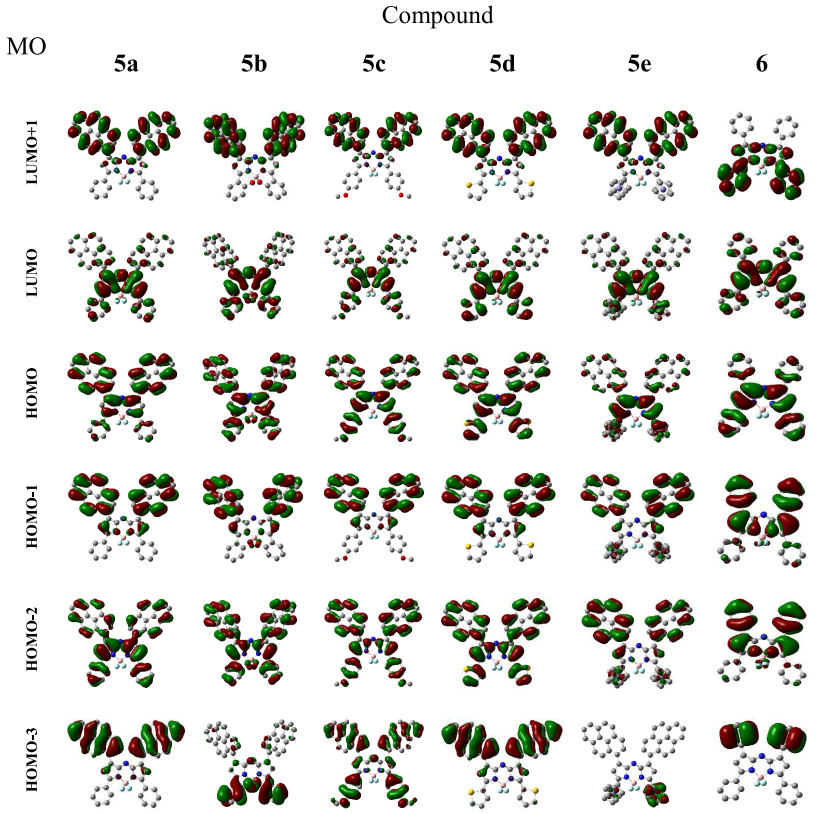

Figure 9. DFT-predicted frontier molecular orbitals for **5a**−**e** and **6**.

contribution from the pyrene fragments to the HOMO, HOMO − 1, and HOMO − 2 of **5a**−**d** is indicative of the potential electron-donating character of the pyrene π-system. This adds partial pyrene-to-aza-BODIPY charge-transfer character to the HOMO → LUMO single-electron excitation and explains significant decrease in fluorescence quantum yields observed in **5a**−**d** when compared to that in **6**. In all compounds studied, pyrene-centered LUMO + 1 and LUMO + 2 were predicted to be ∼1.5 eV higher in energy than the LUMO. In **5e**, the DFT-predicted HOMO is ferrocene-centered, whereas the highest-energy occupied π-type molecular orbital (MO) is HOMO − 1. This electronic structure correlates well with the experimentally observed CV and DPV oxidation of the ferrocene groups in **5e** at low potential. Overall, the DFT-predicted electronic structures of **5a**−**e** are suggestive of a large contribution from the pyrene fragments to the HOMO energy region, which is expected to be exhibited by disappearance of the aza-BODIPY core-centered π−π* transitions observed in the reference compound **6** and appearance of the significant pyrene-to-aza-BODIPY charge-transfer character in transitions observed at the low-energy region of the corresponding UV−vis spectra.

Energies, oscillator strengths, and theoretical UV−vis spectra predicted by the TDDFT calculations for aza-BODIPYs **5a**−**e** and **6** along with experimental UV−vis spectra are shown in Figure 10. In the case of **5a**−**d**, the TDDFT-predicted UV−vis spectra in the low-energy region (550−900 nm) are dominated by three intense bands, which correlate well with the experimental data. Indeed, in the case of **5b**, three bands can be clearly seen in the low-energy region. In the cases of **5c** and **5d**, the most intense band in the 600−720 nm region is accompanied by a lower-intensity broad shoulder, and in the case of **5a**, a broad asymmetric band spans the entire low-energy range. DFT predicts that the lowest-energy transition should be dominated by the HOMO−LUMO single-electron excitation, which has aza-BODIPY/pyrene (π) → aza-BODIPY (π*) character. The other two intense transitions predicted by the TDDFT calculations in the 550−900 nm region are dominated by the pyrene (π, HOMO − 1 and HOMO − 2) → aza-BODIPY (π*, LUMO) excitations. Due to the significant charge-transfer (pyrene-to-aza-BODIPY) character, B3LYP-based TDDFT calculations may overestimate the pyrene-to-aza-BODIPY transition intensities. The predicted locations in energy are in good agreement with the experimental data. In the case of the ferrocene-containing **5e**, TDDFT predicts five transitions with significant MLCT character for the longer-wavelength band experimentally observed between 670 and 1100 nm. These transitions are dominated by HOMO − HOMO − 5 → LUMO single-electron excitations. TDDFT calculations predicted the pyrene-to-pyrene π−π* transitions observed in the UV region. Overall, the TDDFT calculations correctly predicted trends in energies and intensities of the most intense transitions observed experimentally for **5a**−**e**.

Interaction and Potential Complex Formation with Nanocarbon Materials. *Titration with Nanocarbon Materials in Solution.* Installation of the pyrene substituents into **5a**−**e** was motivated by the potential to promote assembly of intermolecular complexes with nanocarbon electron acceptors. The hypothesis that the pyrene motif would successfully provide an effective conduit for association and charge transfer was based on prior reports of other donor−acceptor complexes observed in solution.[151−158] The energetics of electron transfer from the **5a**−**e** photoexcited states to a nanocarbon acceptor can be estimated from the spectroscopic and electrochemical measurements following a standard approach.[159−163] One-electron transfer is energetically favorable in all cases, with ΔG

DOI: 10.1021/acs.jpcc.8b09504
J. Phys. Chem. C 2018, 122, 27893−27916

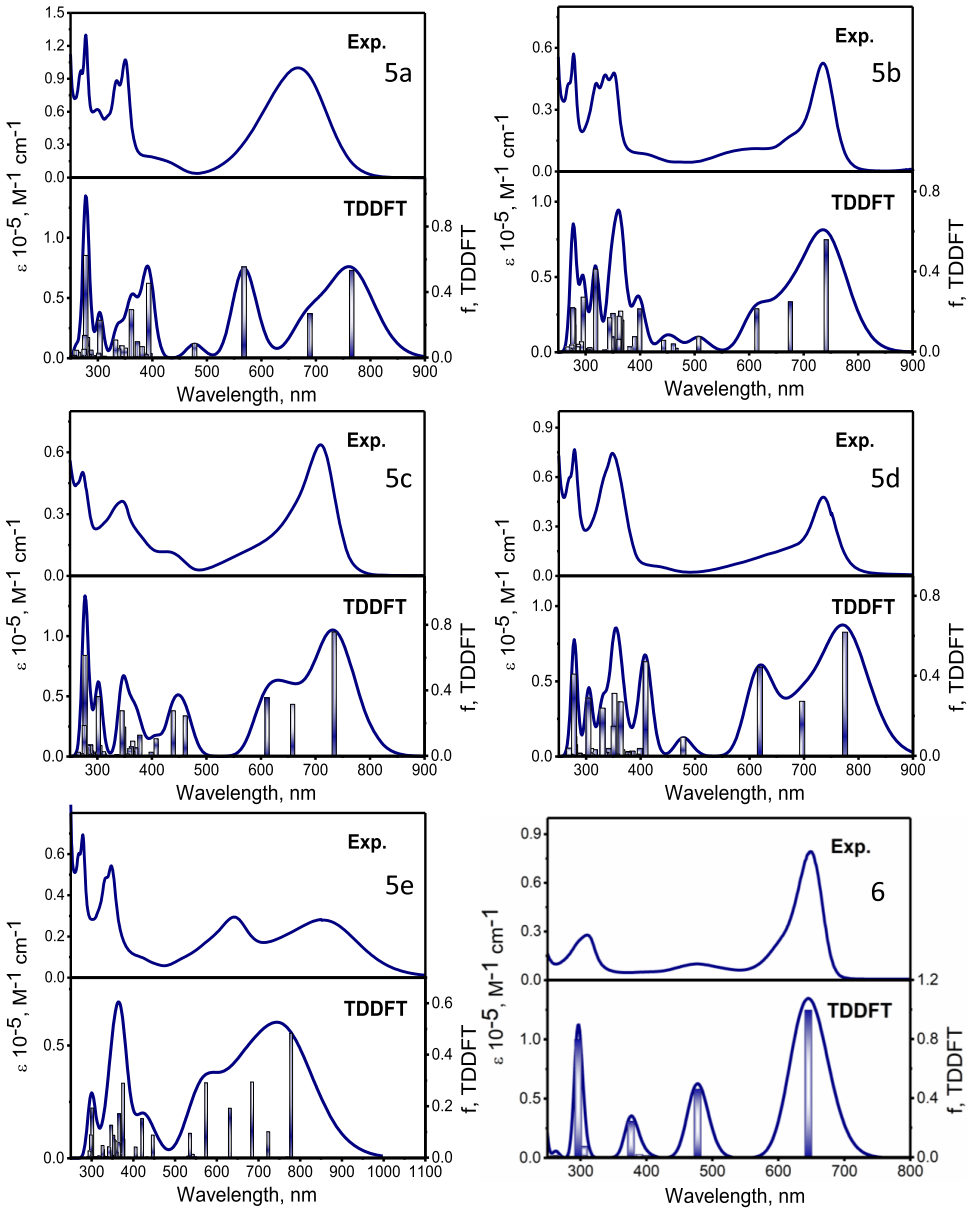

Figure 10. Experimental (top) and TDDFT-predicted (bottom) UV−vis spectra of aza-BODIPYs **5a−e** and **6**.

ranging from −0.2 eV for **5d** to −0.5 eV for **5e**. Changes in static and time-resolved absorption and static fluorescence with addition of C_{60}, C_{70}, (6,5)-SWCNT, and graphene were measured as potential indicators of charge transfer and quantitative evidence of complex formation.

C_{60} and C_{70} Acceptors. Titration of **5a−d** and the reference compound **6** with solutions of C_{60} and C_{70} fullerenes reveals identical results (Figures 11 and S41−S45). No significant reduction in fluorescence was observed with addition of fullerenes when excited at the most intense low-energy band (first excited state). A reduction in both the pyrene and aza-BODIPY emission bands was observed with addition of fullerenes when exciting at 275 and 345 nm. Accounting for the significant absorption at these wavelengths by both C_{60} and C_{70} to first order, a Stern−Volmer analysis of the titrations was carried out taking into consideration a competitive absorption of aza-BODIPY and C_{60}/C_{70} chromophores.[164] The resulting quenching constants are shown in Table 3 and suggest the possibility of weakly associating and/or interacting complexes. However, the need to correct for substantial interference from direct absorption of the fullerenes at these wavelengths[164] when quantifying the reduction in emission leaves significant uncertainty in the evidence for complex formation. The fact that the quenching constants for **5a−e** are smaller or comparable to that for reference **6** demonstrates a lack of any specific enhancement from the pyrene substituents in the formation of complexes at room temperature in solution.

Upon titration of the aza-BODIPYs with fullerenes, all spectral changes in the UV−vis absorption could be accounted for by independent absorption of the added fullerene (Figures 11 and S41−S45). No low-energy absorption bands, characteristic of charge transfer, were observed. The lack of evidence for electron transfer is consistent with recent reports on noncovalent complexes formed between functionalized subphthalocyanines and fullerene.[165−168] We conclude that if there was any residual emission quenching when exciting in the UV region, it was the result of energy transfer rather than charge transfer. Using covalently linked subphthalocyanine−

DOI: 10.1021/acs.jpcc.8b09504
J. Phys. Chem. C 2018, 122, 27893−27916

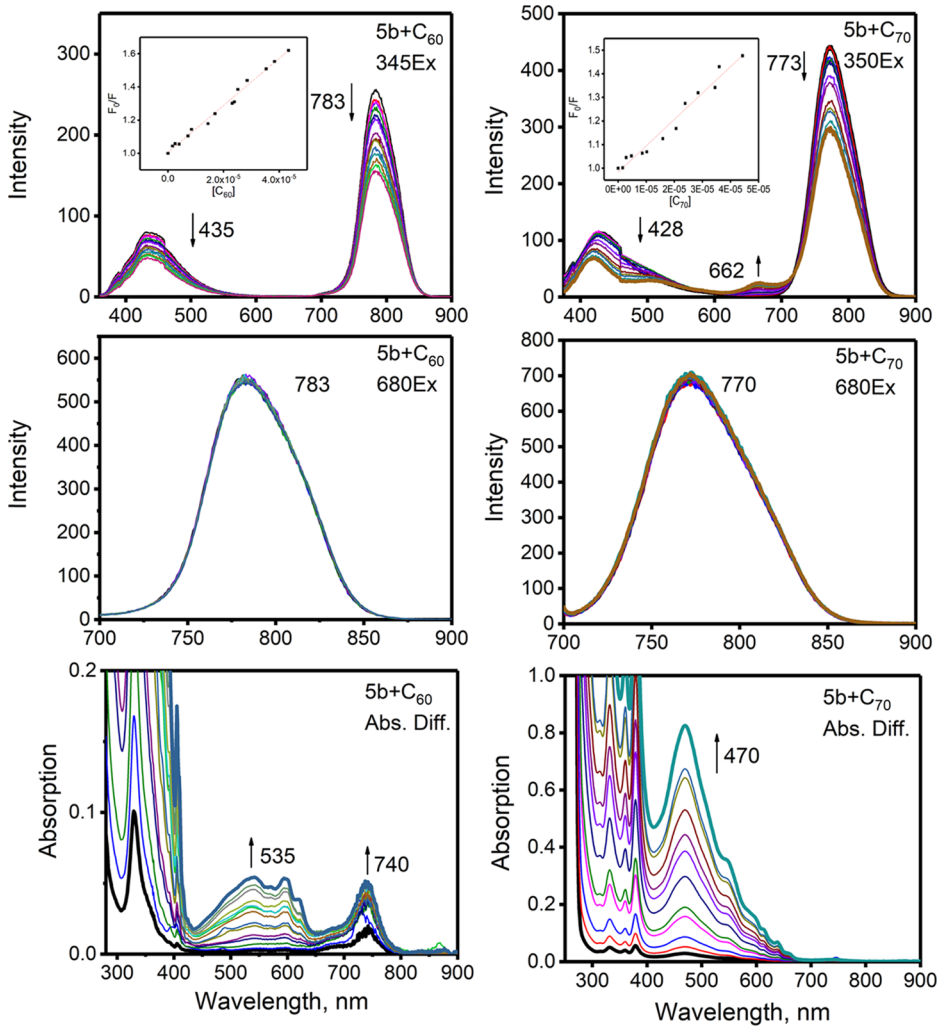

Figure 11. Steady-state (top and middle) and difference absorption (bottom) spectra of the aza-BODIPY **5b** upon stepwise addition of the C_{60} (left panel) and C_{70} (right panel) fullerenes. Excitation wavelengths are shown in the upper right corners of each figure.

Table 3. Estimated Quenching Constants for Complex Formation between 5a–e and 6 and C_{60} or C_{70} Fullerenes[a]

compound	K_{sv} C_{60}	K_{sv} C_{70}
5a	4600	11 500
5b	19 500	15 700
5c	22 900	18 700
5d	9230	15 800
6	12 800	18 200

[a] K_{sv} values were determined using the formula shown in refs159–163.

fullerene dyads, Torres and co-workers demonstrated a strong distance dependence of the donor–acceptor quenching mechanism.[169–171] Shorter distances (~3.1 Å) between the donor and acceptor facilitated electron transfer, whereas small increases in separation (~3.3 Å) favored energy transfer.

Transient absorption was used to investigate the possibility of photoinduced electron transfer between the electron-rich, nonfluorescent **5e** and C_{60}. Figure 12 compares transient absorption for solutions of **5e**, C_{60}, and **5e**/C_{60} (1:10 molar ratio). Transient absorption was measured following excitation at 410 nm, where absorption is a combination of **5e** and C_{60}, and at 650 nm, where the absorption is dominated by **5e**. Figure 12a,b compares excitation at 650 nm with and without C_{60} present. Within the signal-to-noise ratio of the experiments, there was no detectable difference between the shapes or time evolution of the spectra with the addition of C_{60}. The transient spectra are a combination of a ground-state bleach that mirrors the absorption spectrum (negative ΔOD) and excited-state absorption on both the short- and long-wavelength sides of the bleach (positive ΔOD). The spectra appear within the time resolution of the experiment, ~100 fs, and decay in both the visible and near-IR regions of the spectrum with the lifetime reported in Table 1. The absence of electron transfer is supported by the unperturbed decay of the initial excited state of **5e** in the presence of C_{60} and the lack of any new absorption features in the near-IR region consistent with the anion of C_{60}.

When exciting at a shorter wavelength, 410 nm, the transient spectra of **5e** alone are nearly identical to the spectra when exciting at 650 nm. The addition of C_{60} significantly changes the shape and decay of the spectra, Figure 12c, with strong, broad absorption in the near-IR region peaked at around 980 nm. However, the new features are all well accounted for by direct absorption of C_{60}, as presented in Figure 12d. The pump–probe spectra for the 1:10 molar ratio of **5e**/C_{60} are a linear combination of independent **5e** and C_{60} spectra. There is no evidence for charge transfer. We note that transient

DOI: 10.1021/acs.jpcc.8b09504
J. Phys. Chem. C 2018, 122, 27893–27916

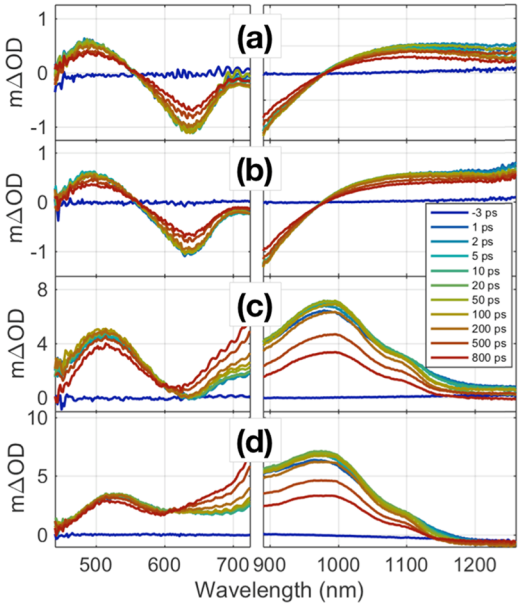

Figure 12. Pump−probe transients for **5e**, a mixture of **5e** and C_{60}, and C_{60} in solution: (a) **5e** excited at 650 nm, (b) **5e**/C_{60} (1:10 mole ratio) excited at 650 nm, (c) **5e**/C_{60} (1:10 mole ratio) excited at 410 nm, and (d) C_{60} excited at 410 nm.

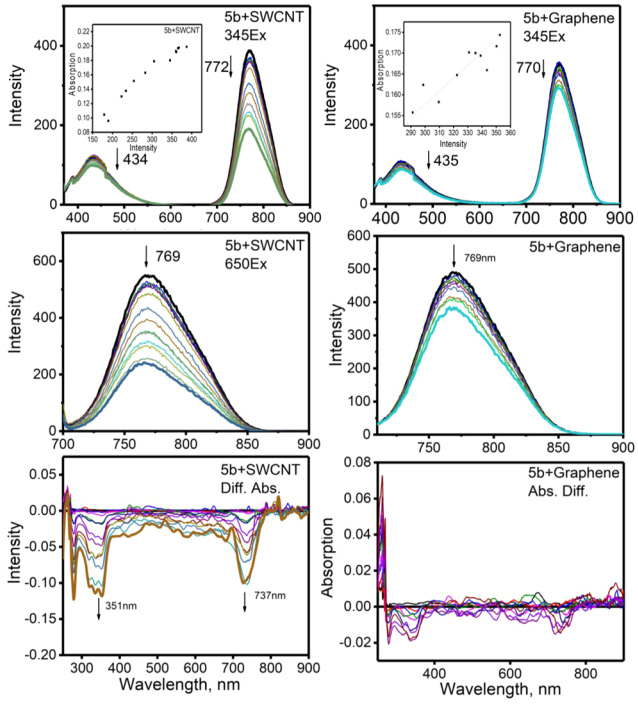

Figure 13. Steady-state emission (top and middle) and difference absorption (bottom) spectra of the aza-BODIPY **5b** upon stepwise addition of the (6,5)-SWCNT (left panel) or graphene (right panel). Excitation wavelengths are shown at the upper right corners of each graph.

absorption features in the near-IR region reported here are very similar to those in other reports that have interpreted the signals as an indicator of energy and charge transfer in analogous systems.[41,42,60,172,173] Our results demonstrate the potential for dominance of the near-IR transient absorption by direct excitation of independent C_{60} in these types of titration studies. This indicates that even at low C_{60} concentrations and longer wavelengths in the tail of the C_{60} absorption, signals originating from direct fullerene absorption must still be carefully accounted for prior to drawing any conclusions associated with energy or charge transfer.

(6,5)-SWCNT and Graphene Acceptors. Titration of aza-BODIPYs **5a−d** and the reference compound lacking the pyrene ligands, **6**, with (6,5)-SWCNT and graphene all resulted in reduction in the observed fluorescence intensity independent of the excitation wavelength (Figures 13 and S46−S50). However, loss of fluorescence was always accompanied by a linearly correlated loss in absorption of the aza-BODIPY, Figures S46−S51. The lack of solubility of (6,5)-SWCNT and graphene complicated the experiments with interference from scattering and changes in the background that limited quantitative confidence when correlating the emission and absorption losses. Within error, the slope of emission versus absorption with addition of SWCNT and graphene was always close to 1. When solutions of **5a−e** and **6** were treated with an excess of (6,5)-SWCNTs or graphene, time-dependent loss of absorption was also observed (Figure S51). We conclude that loss of emission and absorption predominantly reflected removal of the chromophores from the excitation volume via physical adsorption and loss of solubility as SWCNT or graphene was added. The observation indicated association between the aza-BODIPY compounds and the nanocarbon materials. However, there was no observed enhancement in that interaction with installation of the pyrene ligands. The emission and absorption losses were comparable for pyrene-containing **5a−d** and the reference compound **6**. The indirect nature of the measurement, the complexity imposed by the limited solubility of the acceptors, which is likely to change dynamically with donor association, and the potential for larger-scale aggregation limit the interpretation of these observations to the presence of association without characterization of the strength of the interaction.

Solid-State Mixtures. Although there was only minimal evidence for spontaneous association between **5a−e** and fullerenes in solution, assuming some degree of mixing, proximity is forced in the solid state. Several porphyrins and subphthalocyanines have been shown to cocrystallize with C_{60}, forming well-ordered light-harvesting/electron-accepting layers potentially useful for photovoltaic applications.[165−168,174−183] Multilayer combinations of the subphthalocyanines and fullerenes have demonstrated decent photovoltaic performance despite a lack of electron transfer between these components in solution.[184−187] We have compared UV−vis spectra of solid-state samples of **5a−e** with and without equimolar amount of C_{60} (Figures 14 and S52). Peak broadening in some cases did not allow clear observation of cocrystallization with the fullerene. However, in all cases, some interaction between aza-BODIPYs and C_{60} was observed. The clearest examples were **5b** and **5e**, presented in Figure 14. In the case of ferrocene-containing **5e**, the NIR MLCT and visible $\pi-\pi^*$ transitions were shifted to higher energy by ∼30 and ∼10 nm, respectively, in the **5e**·C_{60} complex compared with the same bands in pure **5e**. A shift of ∼20 nm in the opposite direction, to lower energy, was observed in **5b**·C_{60} complexes. Spectral shifts for the other aza-BODIPYs were less evident, Figure S52, and a significant change in the overall absorption profile throughout the longer-wavelength region (550−1000 nm) was found for all systems. These results suggest the possibility of different modes of interactions between **5a−e** and C_{60} that

DOI: 10.1021/acs.jpcc.8b09504
J. Phys. Chem. C 2018, 122, 27893−27916

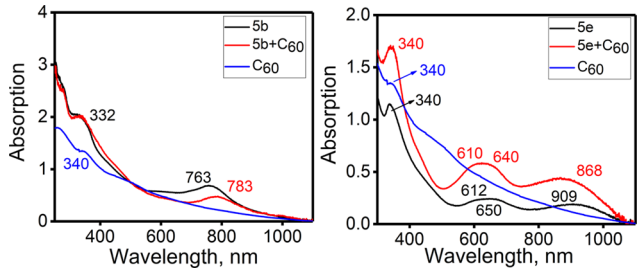

Figure 14. Solid-state (KBr matrix) UV−vis spectra of **5b** and **5e** without and in the presence of C_{60} fullerene. Solid-state spectra of C_{60} fullerene are also provided for comparison.

would not reflect a single favored pyrene−C_{60} chelate interaction motif.

To support our hypothesis, we attempted cocrystallization of equimolar amounts of the individual aza-BODIPYs **5a**−**e** and C_{60} fullerenes. In the majority of cases, the crystals obtained were either too small and/or too poorly diffracting (typically only up to 3 Å), which is common for noncovalent complexes between functional dyes and fullerenes. We were able to obtain relatively good quality crystals suitable for X-ray diffraction for assemblies of **5b**·C_{60} and **5d**·C_{60}. The solid-state structure of **5b**·C_{60} shows formation of a 1:1 complex. The B,O-chelating motif can be clearly seen from the experimental X-ray structure. In addition, a single disordered toluene solvent molecule was also observed in the unit cell (Figure 15). The fullerenes did not form close contacts with the pyrene fragments. Instead, fullerenes were located above the electron-rich B,O-fragment of **5b** and formed a one-dimensional (1D) channeled structure with the closest contact between two C_{60} molecules with a distance of ∼3.87 Å. The closest contact between **5b** and C_{60} was ∼3.34 Å, which is similar to that for noncovalent complexes between subphthalocyanines and C_{60}.[165−168,184−187] The X-ray structure of the noncovalent complex between **5b** and C_{60} also contains intermolecular pyrene−pyrene interactions with short contacts typical of $\pi-\pi$ complexes (∼3.17−3.34 Å). These noncovalent interactions led to the formation of 1D aza-BODIPY chains of **5b**. The pyrene−pyrene intermolecular noncovalent contacts were shorter than expected, and the aza-BODIPY/C_{60} contacts were longer than expected.

Similar to those in the X-ray structure of **5a**, the pyrene fragments in the solid-state structure of **5b**·C_{60} are rotated away from the aza-BODIPY π-system. A general motif in the X-ray structure of noncovalent complexes between **5b** and C_{60} is two independent chains: one consisting of C_{60} and the other of aza-BODIPY **5b** molecules. The electron-deficient fullerenes prefer to interact with the electron-rich part of **5b**, which is localized at the phenolic rather than the pyrenyl fragment of the aza-BODIPY core.

In comparison, crystallization of the equimolar amounts of **5d** and C_{60} fullerene results in the formation of a **5d**·2C_{60} aggregate and characteristic needles of **5d** (Figure 16). A key

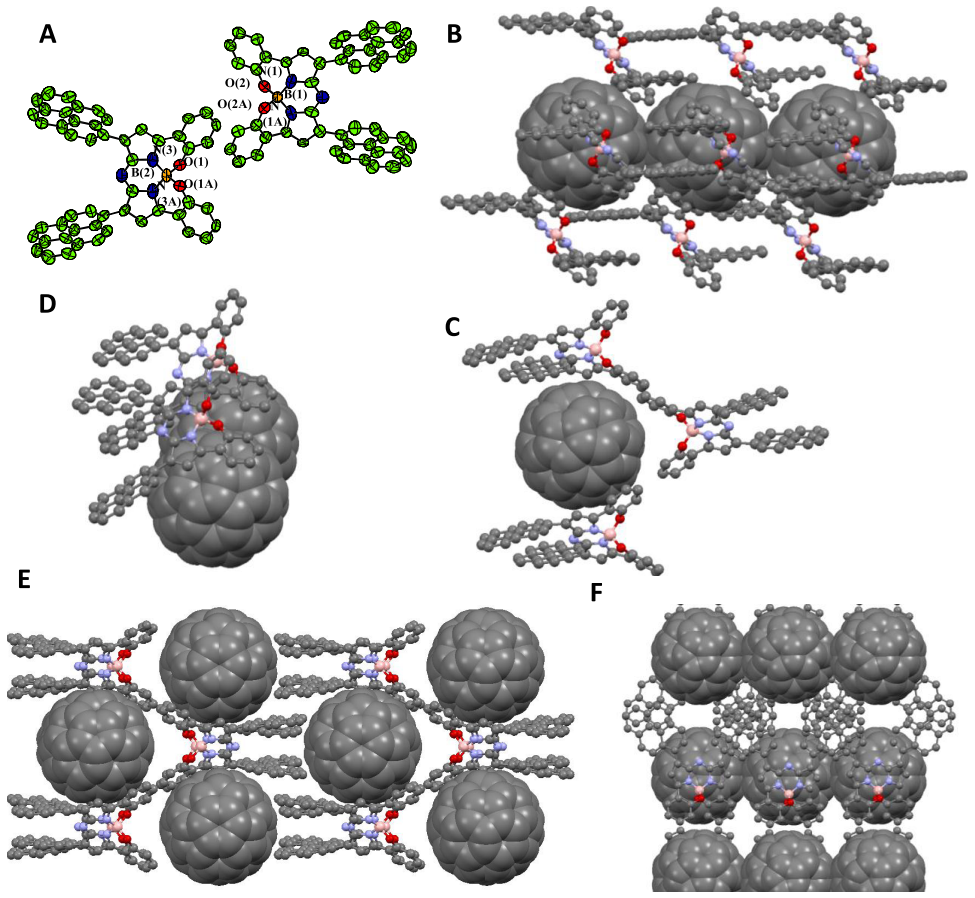

Figure 15. Representative images of the X-ray crystal structure of **5b**·C_{60} (in all cases, hydrogen atoms are omitted for clarity): two independent molecules on **5b** observed in the unit cell; (B) view along the crystallographic *a* axis; (C) C_{60} interacting motif with the electron-rich B,O-chelated area; (D) pyrene−pyrene interaction motif; (E) view along the crystallographic *b* axis; and (F) view along the crystallographic *c* axis.

DOI: 10.1021/acs.jpcc.8b09504
J. Phys. Chem. C 2018, 122, 27893−27916

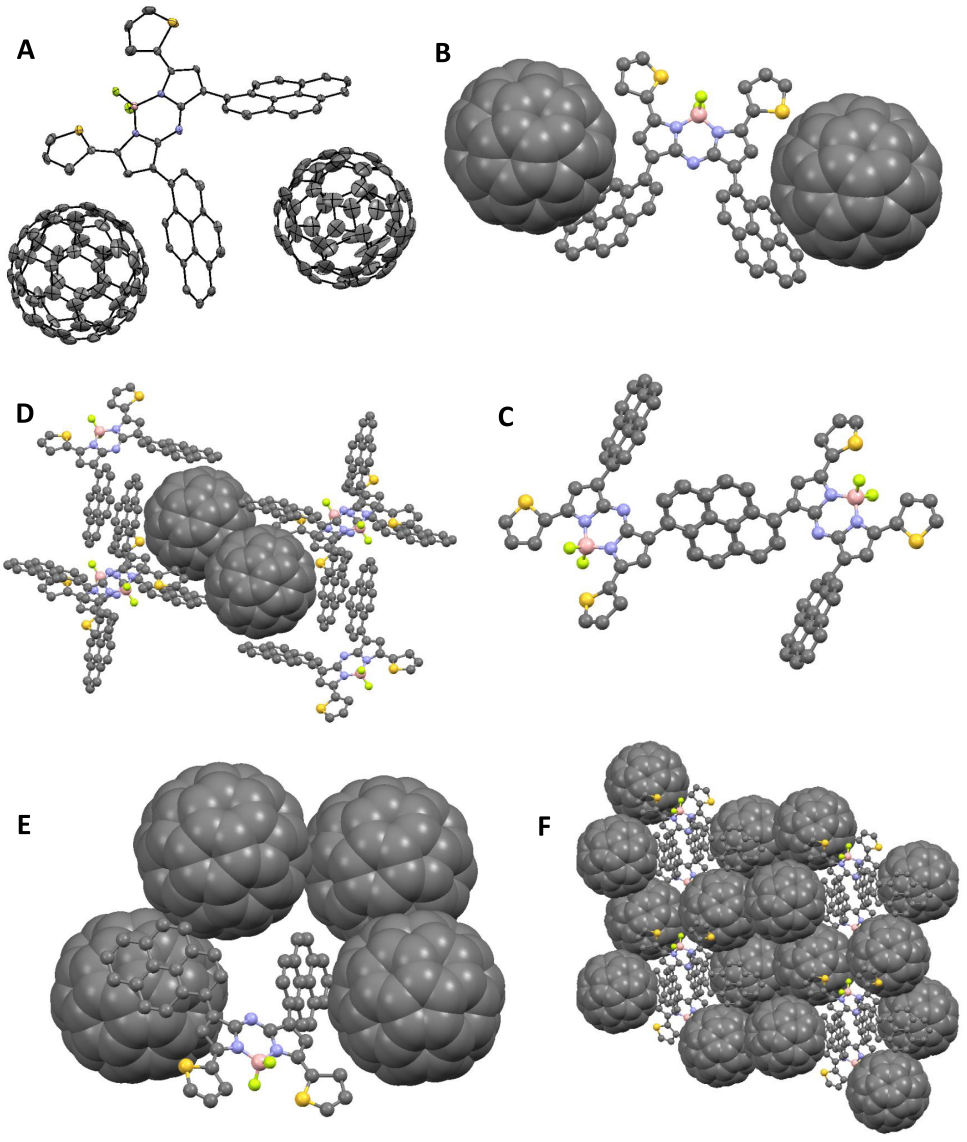

Figure 16. Representative images of the X-ray crystal structure of **5d·2C$_{60}$** (in all cases, hydrogen atoms are omitted for clarity): (A) independent molecules observed in the unit cell; (B) close contacts formed between two fullerene molecules and pyrene fragments in **5d**; (C) pyrene−pyrene interactions in **5d**; (D) "six pyrene−two fullerene" cage; (E) four fullerene molecules forming close contacts around **5d**; and (F) view along the crystallographic *a* axis.

Table 4. DFT-Predicted Interaction Energies for the Formation of Noncovalent Complexes between Pyrene and Nanocarbon Materials[a,b]

functional	pyrene/pyrene	pyrene/C_{60}	pyrene/(6,5)-SWCNT	pyrene/graphene
LC-wPBE	−1.91 (−1.63)	−2.23 (−1.87)	−3.30 (−1.34)	−4.21 (−4.38)
CAM-B3LYP	−1.55 (−1.39)	−1.59 (−1.45)	−2.18 (−1.30)	−2.62 (−2.85)
LC-wPBE-D3	−14.53 (−13.69)	−13.45 (−12.71)	−22.61 (−21.81)	−30.25 (−29.68)
CAM-B3LYP-D3	−10.77 (−10.21)	−10.87 (−10.28)	−17.93 (−17.46)	−23.34 (−22.95)
B3LYP-D3	−12.34 (−11.60)	−11.69 (−11.09)	−20.23 (−18.24)	−26.79 (−26.19)
B97D	−13.31 (−12.33)	−14.00 (−13.75)	−23.26 (−20.71)	−30.03 (−28.99)
wB97XD	−15.94 (−14.68)	−15.41 (−14.60)	−27.49 (−23.23)	−32.34 (−31.45)

[a]Values in parentheses are zero point energy-corrected. [b]All energies in kcal/mol.

difference with the solid-state structure of **5b·C$_{60}$** is the presence of shorter contacts (∼3.1 Å) between the pyrene moieties of **5d** and C_{60}. The aggregate appears to be held together by close pyrene−C_{60} contacts between one **5d** and two fullerenes (∼3.08, 3.31 Å; Figure 16b), with an additional close contact between a third C_{60} and an electron-rich thiophene ring (∼3.32 Å) similar to that in **5b·C$_{60}$**. Each thiophene is situated close to a second C_{60} (∼3.38 Å), though offset at an angle that significantly reduces any $\pi-\pi$ interactions. Pyrene−pyrene interactions (∼3.48 Å) are retained between neighboring molecules of **5d**. One of two pyrene fragments in each **5d** forms a well-aligned H-type

DOI: 10.1021/acs.jpcc.8b09504
J. Phys. Chem. C 2018, 122, 27893−27916

aggregate with a neighboring **5d** molecule (Figure 16c). Six molecules of **5d** form a "cage" around two fullerene molecules (Figure 16d). On the other hand, there are four closely spaced fullerene molecules wrapped around single molecule of **5d** (Figure 16e). The closest contact between two C_{60} molecules is ~3.23 Å, with pairs of fullerenes forming a 2 × 2 ribbon running through the crystal lattice. Overall, X-ray data on **5b·C$_{60}$** and **5d·2C$_{60}$** complexes clearly suggest that the electron density at the BODIPY core can be easily tuned to compete with the pyrene group for noncovalent interaction with the nanocarbon materials. Such competitive interactions can be used to control the desired architecture in noncovalent assemblies formed between aza-BODIPY or BODIPY chromophores and fullerenes.

Density Functional Theory Predictions for Intermolecular Complex Formation. To explore energies for the formation of noncovalent $\pi-\pi$ complexes between pyrene and nanocarbon materials, we have conducted set of DFT calculations for pyrene−pyrene, pyrene−C_{60}, pyrene−(6,5)-SWCNT, and pyrene−graphene assemblies (Table 4, Figures 17 and S53−S58). Because it is expected that the DFT-predicted interaction energies for such weakly interacting complexes should have significant dependence on the exchange-correlation functional, we have compared two functionals that incorporate long-range corrections (CAM-B3LYP[188] and LC-wPBE[189−192]) and several functionals with dispersion corrections (B97D,[193] wB97-XD,[194] CAM-B3LYP-D3,[195] B3LYP-D3,[195] and LC-wPBE-D3;[195] Figures 17 and S53−S58). The DFT-predicted interaction energies for noncovalent pyrene−pyrene dimers show a clear dependence on chosen exchange correlation functional (Table 4). Long-range-corrected functionals predict small interaction energies (~1.4−1.6 kcal/mol) between two pyrene molecules, whereas dispersion-corrected functionals predict higher interaction energies (~10−14 kcal/mol). In all cases, pyrene molecules remained planar and the pyrene−pyrene complexes have slipped-stack geometries (Figures 17 and S53−S58). Geometries also remain planar for the pyrene−graphene complexes calculated by all tested exchange-correlation functionals. Similarly, in the case of pyrene−C_{60} complexes, long-range-corrected functionals predict rather small formation energies (~1.4−1.9 kcal/mol), whereas dispersion-corrected functionals predict much higher interaction energies (~10−13 kcal/mol). It should be noted, however, that dispersion-corrected functionals predict geometries of the pyrene−C_{60} complexes with rather short intermolecular distances, which were not observed in the experimental X-ray structures of the pyrene-containing compounds.[196−199] No difference was predicted by DFT when energies of complex formation for pyrene−pyrene and pyrene−C_{60} pairs were compared between exchange-correlation functionals (on average ±0.5 kcal/mol for each pair). This similarity in energy is indicative of a lack of preference for pyrene−C_{60} over pyrene−pyrene interactions and correlates well with the experimental data. DFT-predicted geometries and interaction energies for the pyrene−(6,5)-SWCNT complexes exhibit the same trends as pyrene−C_{60} complexes. Long-range-corrected functionals predict smaller interaction energies and planar pyrene geometries, whereas dispersion-corrected functionals predict much higher interaction energies and slightly distorted pyrene geometries (Table 4, Figures 17 and S53−S58). When the complex formation energies are compared for pyrene/(6,5)-SWCNT and pyrene/graphene, we found no clear trend across the different exchange-correlation functionals (Table 4). Overall, it seems that the dispersion-corrected functionals overestimate interaction energies for the formation of pyrene−nanocarbon complexes. Such a large interaction, 15−30 kcal/mol, is not consistent with the experimental observations. The DFT calculations predict a lack of the energetic preference for selective pyrene−C_{60} noncovalent complex formation when compared with competing pyrene−pyrene interactions, which correlates well with the experimental X-ray crystal structure of the **5b·C$_{60}$** and **5d·2C$_{60}$** systems. DFT-predicted noncovalent complex formation energies for pyrene−(6,5)-SWCNT and pyrene−graphene were higher, in agreement with the experimental data. Overall, DFT calculations are indicative of weak pyrene−nanocarbon interaction energies that are not strong enough to either facilitate structural assembly or photoinduced electron-transfer processes.

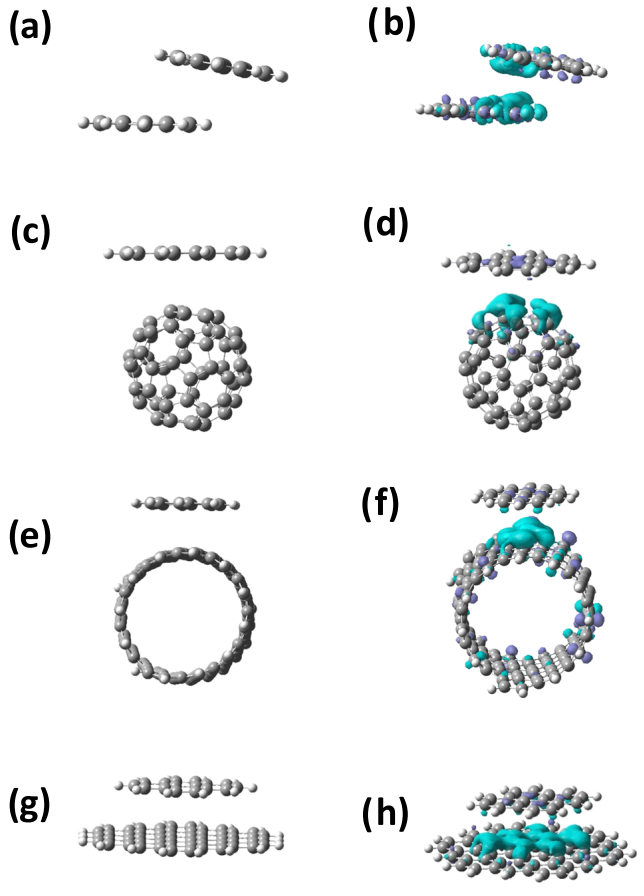

Figure 17. Predicted geometries (a, c, e, g) and charge density isosurfaces (b, d, f, h) of the intramolecular interaction calculated at the LC-wPBE level of theory for pyrene−pyrene (a, b), pyrene−C_{60} (c, d), pyrene−(6,5)-SWCNT (e, f), and pyrene−graphene (g, h), respectively.

CONCLUSIONS

A synthetic strategy was demonstrated for the preparation of a series of 1,7-dipyrene-aza-BODIPY and 1,7-dipyrene-3,5-diferrocene-aza-BODIPY derivatives with pyrene substituents at the β-positions of the aza-BODIPY core. The ability to tune the electronic properties via substitution at the α-positions was demonstrated with full structural and electronic characterization of new aza-BODIPY compounds **5a−e**. Installation of the β-pyrene substituents was motivated by the hypothesis that

DOI: 10.1021/acs.jpcc.8b09504
J. Phys. Chem. C 2018, 122, 27893−27916

they would provide an effective intermolecular binding motif to drive complex formation with nanocarbon-based electron acceptors. This hypothesis was based, in part, on prior reports of analogous applications creating intermolecular charge-transfer complexes that appeared to spontaneously assemble in solution.[1−5,151−158] The intended relative geometry between the two appended pyrenes in **5a−e** was realized as complementary to the curvature of fullerene and SWCNT acceptors, supporting the potential for favorable geometric overlap. Excited-state electron transfer from **5a−e** to the nanocarbon acceptors was shown to be downhill in Gibbs energy. Experiments titrating nanocarbon-based acceptors into solutions of **5a−e** resulted in a significant reduction of measured emission from **5a−e** and the appearance of new absorption features in the transient absorption following photoexcitation, both of which are observations that have been used to support the presence of pyrene-mediated complexation and excited-state electron transfer in analogous systems. However, careful accounting of the interference from direct interaction of the nanocarbon acceptors with the excitation light left only limited, residual evidence of weak interactions with nanocarbon acceptors in solution. No photoinduced electron transfer to the nanocarbon material was observed upon selective excitation of the aza-BODIPY chromophores in solution. Solid-state structures and DFT predictions supported the relatively weak and somewhat nonspecific interaction between **5a−e** and the nanocarbon acceptors. Direct comparison with the control compound lacking pyrene substituents, **6**, demonstrated no significant enhancement in the interaction with nanocarbon acceptors with the addition of the pyrene ligands. The pyrene substituents were demonstrated to be ineffective as a motif to promote and direct intermolecular complex formation with fullerenes and SWCNTs, disproving the initial hypotheses. In the absence of a dominant pyrene−nanocarbon-driven association, tuning of the electron-donating groups at the α-positions of the aza-BODIPY core was observed to play a role in the relatively weak noncovalent complex formation between **5a−e** and fullerenes. This work draws into question conclusions that pyrenes are generally effective ligands in the construction of organic donor−nanocarbon-based-acceptor assemblies, and it highlights the care that must be taken when interpreting some commonly employed approaches to measuring complex formation.

EXPERIMENTAL PART

Reagents and Materials. Solvents were purified using standard approaches: toluene and tetrahydrofuran (THF) were dried over sodium metal, and DCM and chloroform were dried over calcium hydride. Fullerenes C_{60} and C_{70}, (6,5)-SWCNT (95% purity), and graphene were purchased from Sigma-Aldrich. BODIPY derivative **3**,[200] acetyl ferrocene,[201] and chalcones **3a**,[202] **3b**,[203] **3c**,[204] and **3d**[205] were prepared as described earlier. SWCNTs were additionally purified following the literature procedure.[206]

Spectroscopy Measurements. Jasco-720 and Agilent spectrophotometers were used to collect UV−vis data. Fluorescence spectra were recorded on a Cary Eclipse spectrometer. Electrochemical cyclic voltammetry (CV) and differential pulse voltammetry (DPV) measurements were conducted using a CH Instruments electrochemical analyzer utilizing a three-electrode scheme with platinum working, auxiliary, and Ag/AgCl reference electrodes. DCM was used as a solvent, and 0.1 M solution of tetrabutylammonium perchlorate and 0.05 M tetrabutylammonium terakis-(pentafluorophenyl)borate (TFAB) were used as supporting electrolytes. In all cases, experimental redox potentials were corrected using decamethylferrocene (Fc*H) as an internal standard. NMR spectra were recorded on a Varian INOVA instrument with a 500 MHz frequency for protons and 125 MHz frequency for carbons and on a Bruker Avance instrument with a 300 MHz frequency for protons and 75 MHz frequency for carbons. Chemical shifts are reported in parts per million (ppm) and referenced to tetramethylsilane ($Si(CH_3)_4$) as an internal standard. ^{13}C NMR spectra for compounds **4a−d** were not recorded because of the low solubility. High-resolution mass spectra of compounds **4a−e** and **5a−e** were recorded using a Bruker micrOTOF-Q III.

Fluorescence lifetimes were measured using time-correlated single-photon counting (TCSPC). Samples in a 1 cm quartz cuvette were excited with a 650 nm, 40 MHz diode laser (Driver: Picoquant PDL 800-B; Head: Picoquant LDH-P-470). Emission was directed through a double monochromator (Jobin Yvon DH10), detected using an avalanche photodiode (Picoquant MPD PDM), and time-resolved using a TimeHarp 300 TCSPC system. The instrument response of the system is approximately 500 ps full width at half-maximum (FWHM).[207]

Nonemissive samples were measured with pump−probe spectroscopy. A home-built laser system consisting of a Ti:sapphire oscillator (powered by Spectra Physics Millennia Pro) and regenerative amplifier (powered by Spectra Physics Empower 15) generated 75 fs (FWHM), 0.8−1.0 mJ, 815 nm pulses at a repetition rate of 1 kHz. A portion of this light was directed into a home-built noncollinear optical parametric amplifier to create excitation pulses at 640, 650, and 920 nm. Continuum probe pulses of 420−750 and 850−1400 nm were created by focusing a small fraction of the 815 nm light (~20 μW) into a 2 mm sapphire window and yttrium aluminum garnet crystal, respectively. The excitation light was polarized at 54.7° relative to the probe polarization (the magic angle) to isolate the isotropic dynamics of the excited state. Time delay between the excitation and probe pulses was controlled by a mechanical delay stage (Newport UTM150PP.1). Pump and probe pulses were focused and spatially overlapped in a 1 mm quartz cuvette containing the sample. The probe beam emerging from the sample was collimated, directed through a monochromator, and detected on an array. A Princeton Instruments SP2150i monochromator (150 lines/mm, 500 nm blaze) with an attached 256 pixel diode array (Hamamatsu S3902-256Q) was used for visible light. A Princeton Instruments SP2150 monochromator (150 lines/mm, 1200 nm blaze) with an attached 256 linear pixel InGaAs diode array (Hamamatsu G9213-256S) was used for infrared light. The pump beam was modulated at half the laser repetition rate, whereas the probe beam was measured for every laser pulse, and the change in optical density, ΔOD, induced by the pump was calculated and recorded for each pulse pair. Typically, 20 000−40 000 pulse pairs were averaged for each time point presented in the pump−probe data. The dependence of the ΔOD signal for pump pulse energies between 20 and 100 nJ was found to be linear. Data shown was collected with pump pulse energies of 60 and 120 nJ. Samples had an optical density of <0.25 at the excitation wavelength and were held in a 1 mm path length cell during data collection. Absorption spectra taken before and after the pump−probe experiments were

DOI: 10.1021/acs.jpcc.8b09504
J. Phys. Chem. C 2018, 122, 27893−27916

indistinguishable, indicating no evidence of sample degradation.

Computational Details. The starting geometries of compounds **5a**–**e** and **6** were optimized using a B3LYP exchange-correlation functional.[208,209] The B3LYP exchange-correlation functional was found to result in good agreement between calculated and experimentally determined bond distances and angles in ferrocene-containing compounds.[210−215] Energy minima in optimized geometry were confirmed by the frequency calculations (absence of the imaginary frequencies). The solvent effect was calculated using the polarized continuum model (PCM).[216] In all calculations, DCM was used as the solvent. In PCM-TDDFT calculations, the first 50 states were calculated. Full-electron Wachter's basis set[217] was utilized for iron atoms, whereas all other atoms were modeled using the 6-311G(d)[218] basis set. Gaussian 09 software was used in all calculations.[219] The QMForge program was used for molecular orbital analysis.[220] In DFT calculations on the formation energies of pyrene−pyrene, pyrene−C_{60}, pyrene−(6,5)-SWCNT, and pyrene−graphene noncovalent complexes, long-range-corrected CAM-B3LYP and LC-wPBE exchange-correlation functionals and several functionals with dispersion correction (B97D, wB97XD CAM-B3LYP-D3, and LC-wPBE-D3) have been tested. For pyrene−pyrene, pyrene−C_{60}, pyrene−(6,5)-SWCNT, and pyrene−graphene systems, the 6-31+G(d) basis set was used for all atoms. (6,5)-SWCNT was modeled by the 134-atom truncated geometry with terminal hydrogen atoms located at the edges. The length of such a (6,5)-SWCNT model was 13.568 Å, which is sufficient for an accurate description of pyrene−(6,5)-SWCNT interactions. Graphene was modeled by the repeated translation of the six-membered carbon units (54 total carbon atoms). The terminal carbon atoms in the graphene model were terminated by hydrogens. The final model had a 14.48 × 14.48 $Å^2$ size, which is sufficient to model pyrene−graphene interactions.

X-ray Crystallography. Single crystals of aza-BODIPYs **4e**, **5a**, **5d**, and **5e** and **5b·C_{60}** and **5d·2C_{60}** complexes suitable for X-ray crystallographic analysis were obtained by slow evaporation from their DCM (**4e**, **5a**, **5d**, and **5e**) or DCM/toluene (**5b·C_{60}**, and **5d·2C_{60}**) solutions. X-ray diffraction data for **5a** and **5b·C_{60}** were collected on a Rigaku RAPID II Image Plate system using graphite-monochromated Cu Kα radiation (λ = 1.54187 Å) at 123 K. Data for **5d**, **5e**, and **5d·2C_{60}** compounds were obtained on a Bruker D8 QUEST ECO CMOS diffractometer using graphite-monochromated Mo Kα radiation (λ = 0.71073 Å) at 150 K. Data for **4e** were obtained on a Bruker APEX-II diffractometer using graphite-monochromated Cu Kα radiation (λ = 1.54187 Å) at 150 K. All diffractometer manipulations, including data collection, integration, and scaling, were carried out using the Bruker APEX3 software suite. Absorption corrections were applied using SADABS. The structures were solved by direct methods[221] (**5a**, **5d**, **5e**, **5d·2C_{60}**) or by the SuperFlip method[222,223] (**5b·C_{60}**) and refined by full-matrix least-squares refinement using Crystals for Windows[224] (**5a**) or SHELXL-2014/7[225−227] (**5b·C_{60}**, **5d**, **5e**, **5d·2C_{60}**) programs. No obvious missed symmetry was reported by PLATON. All nonhydrogen atoms were refined with anisotropic thermal parameters. Hydrogen atoms were placed in idealized positions and refined using a riding model. The solvent toluene molecule in the **5b·C_{60}** complex was found to be disordered over two sites. In **5d·2C_{60}**, the disorder in one of two C_{60} molecules in the asymmetric unit could not be satisfactorily modeled, leading to higher than desirable thermal parameters for the carbon sites in this unit. A "flip"-type disorder was observed for thiophenyl side chains in **5d** and **5d·2C_{60}**, wherein different types of atoms (sulfur and carbon) occupy positions that are close to each other. This disorder influences the thermal parameters of the respective sulfur and carbon atoms, which were therefore equated for each pair of disordered atoms in the disordered rings.

Crystal data for **4e** $C_{60}H_{39}Fe_2N_3$: molecular weight (MW) = 913.64, monoclinic, space group $P2_1/n$, a = 7.3960(4) Å, b = 45.697(3) Å, c = 12.5412(7) Å, α = 90°, β = 94.623(5)°, γ = 90°, V = 4224.82 $Å^3$, Z = 4, μ = 5.864 mm^{-1}, 35 657 reflections ($3810I > 2\sigma(I)$), $2\theta_{max}$ = 125.54; final R_1 = 0.0845, R_w (all) = 0.1494. Crystal data for **5a** $C_{52}H_{30}B_1F_2N_3$: MW = 745.64, monoclinic, space group $P2_1/c$, a = 12.8265(2) Å, b = 20.1233(4) Å, c = 14.4166(10) Å, α = 90°, β = 105.552(7)°, γ = 90°, V = 3584.9(2) $Å^3$, Z = 4, μ = 0.697 mm^{-1}, 12 889 reflections ($1665I > 2\sigma(I)$), $2\theta_{max}$ = 58.935; final R_1 = 0.0782, R_w (all) = 0.1874. Crystal data for **5b•C_{60}** $C_{119}H_{36}B_1O_2N_3$: MW = 1458.28, monoclinic, space group C_2/c, a = 19.7995(4) Å, b = 47.3003(9) Å, c = 14.7939(10) Å, α = 90°, β = 106.263(7)°, γ = 90°, V = 13300.4(11) $Å^3$, Z = 8, μ = 0.677 mm^{-1}, 6927 reflections ($3569I > 2\sigma(I)$), $2\theta_{max}$ = 50.427; final R_1 = 0.1203, R_w (all) = 0.2665. Crystal data for **5d** $C_{49}H_{28}BCl_2F_2N_3S_2$: MW 842.57, monoclinic, space group $P2_1/c$, a = 29.1647(15) Å, b = 7.7468(3) Å, c = 33.4875(16) Å, α = 90°, β = 96.487(3)°, γ = 90°, V = 7517.5(6) $Å^3$, Z = 8, μ = 0.337 mm^{-1}, 12 828 reflections ($6009I > 2\sigma(I)$), $2\theta_{max}$ = 49.556; final R_1 = 0.0966, wR_2 (all) = 0.1880. Crystal data for **5d•C_{60}** $C_{169}H_{26}BF_2N_3OS_2$: MW = 2226.86, triclinic, space group $P\bar{1}$, a = 13.2973(10) Å, b = 16.7957(12) Å, c = 22.0745(16) Å, α = 101.739(4)°, β = 105.539(3)°, γ = 99.699(4)°, V = 4518.7(6) $Å^3$, Z = 2, μ = 0.143 mm^{-1}, 15 469 reflections ($7504I > 2\sigma(I)$), $2\theta_{max}$ = 49.658; final R_1 = 0.1075, wR_2 (all) = 0.2836. Crystal data for **5e** $C_{60}H_{38}BF_2Fe_2N_3$: MW = 961.44, monoclinic, space group $P2_1/c$, a = 21.490(2) Å, b = 9.7500(10) Å, c = 19.997(2) Å, α = 90°, β = 96.947(4)°, γ = 90°, V = 4159.2(7) $Å^3$, Z = 4, μ = 0.756 mm^{-1}, 7127 reflections ($4418I > 2\sigma(I)$), $2\theta_{max}$ = 49.514; final R_1 = 0.1036, wR_2 (all) = 0.2078. Additional crystallographic information for all compounds may be found in the combined CIF included as the Supporting Information or accessible from the Cambridge Structural Database: CCDC-1582584 (**5a**), CCDC-1582586 (**5d**), CCDC-1582588 (**5e**), CCDC-1582585 (**5b·C_{60}**), and CCDC-1582587 (**5d·2C_{60}**).

EXPERIMENTAL PROCEDURE

Compound 2e. To the solution of acetyl ferrocene (8.7 mmol, 2000 mg) and pyrenecarboxaldehyde (8.7 mmol, 2017 mg) in dry dimethylformamide (20 mL), sodium hydride (8.7 mmol, 209 mg) was added portionwise. The resulting mixture was stirred for 5 min at room temperature and then quenched with iced water (20 mL). The resulting precipitate was filtered, washed with water, and dried. Yield 3600 mg (90%). ^{1}H NMR (300 MHz, $CDCl_3$) δ 8.99 (d, $J_{H,H}$ = 15.6 Hz, 1H), 8.64 (d, $J_{H,H}$ = 9.3 Hz, 1H), 8.44 (d, $J_{H,H}$ = 8.0 Hz, 1H), 8.26−8.21 (m, 4H), 8.16−8.02 (m, 3H), 7.44 (d, $J_{H,H}$ = 15.6 Hz, 1H), 5.02−5.01 (m, 2H), 4.65−4.64 (m, 2H), 4.28 (s, 5H); ^{13}C NMR (75 MHz, $CDCl_3$) δ 137.73, 132.79, 131.53, 130.98, 130.38, 129.38, 128.72, 128.66, 127.50, 126.46, 126.07, 125.95, 125.49, 125.16, 124.24, 123.01, 81.03, 73.00, 70.32, 69.99.

DOI: 10.1021/acs.jpcc.8b09504
J. Phys. Chem. C 2018, 122, 27893−27916

Compound 3a. To the solution of compound **2a** (2.69 mmol, 896 mg) in nitromethane (10 mL), 1,8-diazabicyclo[5.4.0]undec-7-ene (DBU) (2.69 mmol, 410 mg) was added. The resulting mixture was refluxed for 5 min. The resulting colorless solution was cooled down to room temperature and diluted with water (10 mL), and then, methanol was added until white solid precipitated. The product was collected by filtration, yielding 990 mg (93%) of **3a**. ^{1}H NMR (500 MHz, $CDCl_3$) δ 8.51 (d, $J_{H,H}$ = 9.4 Hz, 1H), 8.23−8.20 (m, 3H), 8.17 (d, $J_{H,H}$ = 8.0 Hz, 1H), 8.09 (d, $J_{H,H}$ = 11.6 Hz, 1H), 8.05−8.01 (m, 2H), 7.95−7.93 (m, 3H), 7.58−7.55 (m, 1H), 7.46−7.43 (m, 2H), 5.52−5.47 (m, 1H), 5.08 (dd, $J_{H,H}$ = 12.6, 7.0 Hz, 2H), 3.76 (dd, $J_{H,H}$ = 6.8, 3.1 Hz, 2H); ^{13}C NMR (75 MHz, $CDCl_3$) δ 197.05, 136.49, 133.74, 132.61, 131.51, 130.96, 130.87, 128.89, 128.78, 128.21, 127.90, 127.39, 126.36, 125.72, 125.49, 125.26, 122.04, 79.59, 42.15.

Compound 3b. To the solution of compound **2b** (4.02 mmol, 1400 mg) in nitromethane (15 mL), DBU (4.02 mmol, 611 mg) was added. The resulting mixture was stirred for 10 min at room temperature. Then, the resulting colorless solution was acidified with acetic acid (1 mL) and diluted with water. The product was extracted with chloroform. The organic layer was washed with water (2 × 40 mL) and brine solution, dried over $MgSO_4$, and evaporated to dryness, yielding 1478 mg (89%) of pure **3b**. ^{1}H NMR (500 MHz, $CDCl_3$) δ 11.85 (s, 1H), 8.43 (d, $J_{H,H}$ = 9.3 Hz, 1H), 8.18−8.14 (m, 3H), 8.11 (d, $J_{H,H}$ = 8.0 Hz, 1H), 8.03 (d, $J_{H,H}$ = 8.9 Hz, 1H), 7.99−7.95 (m, 2H), 7.86 (d, $J_{H,H}$ = 8.0 Hz, 1H), 7.70 (dd, $J_{H,H}$ = 8.1, 1.5 Hz, 1H), 7.42−7.38 (m, 1H), 6.89−6.88 (m, 1H), 6.83−6.80 (m, 1H), 5.44−5.39 (m, 1H), 4.99 (dd, $J_{H,H}$ = 11.8, 6.5 Hz, 2H), 3.78 (dd, $J_{H,H}$ = 17.8, 6.5 Hz, 2H); ^{13}C NMR (75 MHz, $CDCl_3$) δ 202.73, 162.62, 136.99, 132.05, 131.47, 131.01, 130.79, 129.66, 128.87, 128.78, 127.97, 127.34, 126.40, 125.80, 125.54, 125.42, 125.26, 124.86, 123.31, 121.83, 119.25, 119.18, 118.87, 79.51, 41.53, 29.85.

Compound 3c. To the solution of compound **2c** (1.82 mmol, 660 mg) in nitromethane (10 mL), DBU (1.82 mmol, 276 mg) was added. The resulting mixture was stirred for 10 min at room temperature. Then, the resulting colorless solution was diluted with water and the product was extracted with chloroform. The organic layer was dried over $MgSO_4$ and evaporated to dryness, yielding 694 mg (90%) of pure **3c**. ^{1}H NMR (300 MHz, $CDCl_3$) δ 8.52 (d, $J_{H,H}$ = 9.4 Hz, 1H), 8.23−8.14 (m, 4H), 8.00−8.004 (m, 3H), 7.96−7.91 (m, 3H), 6.93−6.88 (m, 2H), 5.52−5.43 (m, 1H), 5.09 (dd, $J_{H,H}$ = 12.6, 6.8 Hz, 2H), 3.85 (s, 3H), 3.70−3.67 (m, 2H); ^{13}C NMR (75 MHz, $CDCl_3$) δ 195.48, 163.99, 132.84, 131.49, 130.88, 130.86, 130.51, 129.57, 128.83, 128.70, 127.83, 127.39, 126.32, 125.66, 125.44, 125.23, 124.93, 79.60, 55.68, 41.77.

Compound 3d. To the solution of compound **2d** (3.50 mmol, 1193 mg) in nitromethane (15 mL). DBU (3.50 mmol, 532 mg) was added. The resulting mixture was stirred for 10 min at room temperature. Then, the resulting colorless solution was diluted with water and the product was extracted with chloroform. The organic layer was dried over $MgSO_4$ and evaporated to dryness, yielding 1281 mg (91%) of pure **3d**. ^{1}H NMR (300 MHz, $CDCl_3$) δ 8.50 (d, $J_{H,H}$ = 9.4 Hz, 1H), 8.23−8.15 (m, 4H), 8.09−8.00 (m, 3H), 7.95 (d, $J_{H,H}$ = 8.0 Hz, 1H), 7.71−7.70 (m, 1H), 7.64−7.62 (m, 1H), 7.11−7.08 (m, 1H), 5.50−5.41 (m, 1H), 5.13 (dd, $J_{H,H}$ = 12.6, 6.9 Hz, 2H), 3.74−3.70 (m, 2H); ^{13}C NMR (75 MHz, $CDCl_3$) δ 189.85, 143.61, 134.48, 132.42, 132.28, 131.47, 130.96, 130.83, 128.82, 128.78, 128.37, 127.90, 127.36, 126.35, 125.72, 125.49, 125.41, 125.24, 124.89, 123.43, 121.97, 79.40, 42.70.

Compound 3e. To the solution of compound **2e** (8.10 mmol, 3580 mg) in nitromethane (25 mL), DBU (8.10 mmol, 1230 mg) was added. The resulting mixture was refluxed for 10 min. The resulting colorless solution was cooled down to room temperature and diluted with water (20 mL), and the product was extracted with chloroform, washed with water and brine, dried over Na_2SO_4, and evaporated to dryness. Yield 3260 mg (80%) of **3e**. ^{1}H NMR (300 MHz, $CDCl_3$) δ 8.57 (d, $J_{H,H}$ = 9.4 Hz, 1H), 8.26−8.19 (m, 4H), 8.09−7.96 (m, 4H), 5.48−5.39 (m, 1H), 5.12 (dd, $J_{H,H}$ = 12.6, 7.0 Hz, 2H), 4.77−4.73 (m, 2H), 4.49−4.48 (m, 2H), 4.01 (s, 5H), 3.57 (dd, $J_{H,H}$ = 17.5, 6.3 Hz, 2H); ^{13}C NMR (75 MHz, $CDCl_3$) δ 201.05, 132.89, 131.53, 130.97, 130.91, 128.95, 128.77, 127.90, 127.41, 126.36, 125.71, 125.49, 125.18, 124.97, 122.21, 79.61, 78.51, 72.73, 72.69, 69.95, 69.41, 43.11.

General Procedure for the Synthesis of Compounds 4a−e. The mixture of appropriate nitrobutanone derivative **3a−d** and ammonium acetate (50 equiv) was refluxed in ethanol or *n*-butanol (30 mL) for 12−24 h. After cooling to room temperature, the precipitate was filtered, washed with ethanol, and dried.

*Compound **4a**.* The mixture was refluxed for 24 h. Yield 280 mg (35%). ^{1}H NMR (500 MHz, $CDCl_3$) δ 8.53 (d, $J_{H,H}$ = 9.4 Hz, 2H), 8.18 (d, $J_{H,H}$ = 7.6 Hz, 2H), 8.15−8.13 (m, 2H), 8.10−8.06 (m, 6H), 7.98−7.95 (m, 6H), 7.81 (d, $J_{H,H}$ = 8.9 Hz, 2H), 7.69 (d, $J_{H,H}$ = 7.6 Hz, 2H), 7.63−7.60 (m, 4H), 7.55−7.52 (m, 2H), 7.38 (s, 2H); HRMS (atmospheric pressure chemical ionization (APCI) positive) calcd for $C_{52}H_{31}N_3$ $[M + H]^+$: 698.2591, found 698.2575.

*Compound **4b**.* The mixture was refluxed for 12 h. Yield 330 mg (25%). ^{1}H NMR (300 MHz, dimethyl sulfoxide-d_6) δ 8.41 (d, $J_{H,H}$ = 9.3 Hz, 1H), 8.26−8.25 (m, 2H), 8.22−8.18 (m, 4H), 8.12−8.05 (m, 8H), 7.81 (d, $J_{H,H}$ = 9.1 Hz, 2H), 7.75 (s, 1H), 7.69−7.68 (m, 1H), 7.43−7.40 (m, 2H), 7.21−7.19 (m, 2H), 7.08−7.05 (m, 2H); HRMS (APCI positive) calcd for $C_{52}H_{31}N_3O_2$ $[M + H]^+$: 730.2489, found 730.2459.

*Compound **4c**.* The mixture was refluxed for 12 h. Yield 182 mg (27%). ^{1}H NMR (300 MHz, $CDCl_3$) δ 8.54 (d, $J_{H,H}$ = 9.3 Hz, 2H), 8.19 (d, $J_{H,H}$ = 7.9 Hz, 2H), 8.14−8.11 (m, 2H), 8.07−7.93 (m, 12H), 7.80 (d, $J_{H,H}$ = 8.9 Hz, 2H), 7.68 (d, $J_{H,H}$ = 7.9 Hz, 2H), 7.29 (s, 2H), 7.14 (d, $J_{H,H}$ = 8.7 Hz, 4H), 3.96 (s, 6H); HRMS (APCI positive) calcd for $C_{54}H_{35}N_3O_2$ $[M + H]^+$: 758.2802, found 758.2782.

*Compound **4d**.* The mixture was refluxed for 20 h in *n*-butanol. Yield 166 mg (26%). ^{1}H NMR (300 MHz, $CDCl_3$) δ 8.51 (d, $J_{H,H}$ = 9.2 Hz, 2H), 8.16−8.12 (m, 7H), 8.08−8.03 (m, 4H), 7.99−7.95 (m, 7H), 7.80−7.77 (m, 2H), 7.71−7.70 (m, 1H), 7.68−7.65 (m, 2H), 7.60−7.58 (m, 1H); HRMS (APCI positive) calcd for $C_{48}H_{27}N_3S_2$ $[M + H]^+$: 710.1719, found 710.1698.

*Compound **4e**.* The mixture was refluxed for 24 h in *n*-butanol under an argon atmosphere. After cooling to room temperature, the product was filtered, washed with ethanol, and dried. The crude product was purified by column chromatography on Al_2O_3 using toluene as the solvent. The dark violet fraction was collected and evaporated to dryness, yielding 260 mg (15%) of pure **4e**. ^{1}H NMR (300 MHz, $CDCl_3$) δ 8.56 (d, $J_{H,H}$ = 9.3 Hz, 2H), 8.23 (d, $J_{H,H}$ = 8.0 Hz, 2H), 8.14 (d, $J_{H,H}$ = 7.4 Hz, 2H), 8.08 (d, $J_{H,H}$ = 6.9 Hz, 2H), 7.98−7.93 (m, 6H), 7.83 (d, $J_{H,H}$ = 8.9 Hz, 2H), 7.72 (d, $J_{H,H}$ = 8.0 Hz, 2H), 6.98 (s, 2H), 4.99 (t, $J_{H,H}$ = 1.9 Hz, 4H), 4.68 (t,

DOI: 10.1021/acs.jpcc.8b09504
J. Phys. Chem. C 2018, 122, 27893−27916

$J_{H,H}$ = 1.9 Hz, 4H), 4.33 (s, 10H); ^{13}C NMR (75 MHz, $CDCl_3$) δ 156.45, 150.41, 140.97, 131.48, 131.08, 130.65, 129.75, 129.72, 129.31, 127.59, 127.35, 127.02, 126.25, 125.84, 125.05, 125.01, 124.95, 124.72, 124.28, 119.38, 71.48, 70.52, 69.81, 67.92; HRMS (APCI positive) calcd for $C_{60}H_{39}Fe_2N_3$ $[M + H]^+$: 914.1919, found 914.1889.

Compound ***5a***. The solution of compound **4a** (0.143 mmol, 100 mg) in DCM (10 mL) was treated with *N*,*N*-diisopropylethylamine (DIPEA) (0.717 mmol, 92 mg) and stirred for 10 min at room temperature. Then, the solution of $BF_3{\cdot}Et_2O$ (1.43 mmol, 203 mg) was added dropwise and the mixture was stirred overnight at room temperature. Then, the reaction mixture was slowly quenched with methanol (10 mL) and the resulting precipitate was filtered, yielding 87 mg (81%) of pure dye **5a**. ^{1}H NMR (500 MHz, $CDCl_3$) δ 8.58 (d, $J_{H,H}$ = 9.3 Hz, 2H), 8.26 (d, $J_{H,H}$ = 8.0 Hz, 2H), 8.21−8.20 (m, 4H), 8.18−8.16 (m, 4H), 8.09 (d, $J_{H,H}$ = 9.3 Hz, 2H), 8.04−8.00 (m, 4H), 7.90−7.87 (m, 4H), 7.58−7.55 (m, 6H), 7.27 (m, 2H); ^{13}C NMR (75 MHz, $CDCl_3$) δ 131.87, 131.79, 131.42, 131.20, 130.95, 129.97, 129.84, 128.91, 128.44, 128.13, 127.50, 126.24, 125.78, 125.54, 125.44, 124.79, 124.55; HRMS (APCI positive) calcd for $C_{52}H_{30}BF_2N_3$ $[M + H]^+$: 746.2560, found 746.2433.

Compound ***5b***. The solution of compound **4b** (0.137 mmol, 100 mg) in dry THF (10 mL) was treated with DIPEA (2.05 mmol, 264 mg) and stirred for 10 min at room temperature. Then, the solution of $BF_3{\cdot}Et_2O$ (2.74 mmol, 390 mg) was added dropwise and the mixture was stirred overnight at room temperature. Then, the reaction mixture was slowly quenched with water (20 mL) and the product was extracted with EtOAc, dried over Na_2SO_4, and evaporated to dryness. The crude product was purified by column chromatography on silica gel using toluene as the solvent, yielding 20 mg (20%) of pure dye **5b**. ^{1}H NMR (500 MHz, $CDCl_3$) δ 8.68 (d, $J_{H,H}$ = 9.3 Hz, 2H), 8.34 (d, $J_{H,H}$ = 8.0 Hz, 2H), 8.22−8.18 (m, 4H), 8.16 (d, $J_{H,H}$ = 9.3 Hz, 2H), 8.06−7.94 (m, 10H), 7.52−7.58 (m, 2H), 7.44 (s, 2H), 7.22−7.15 (m, 4H); ^{13}C NMR (75 MHz, $CDCl_3$) δ 156.08, 142.96, 133.74, 131.82, 131.45, 131.00, 129.79, 129.70, 129.11, 128.35, 128.04, 127.72, 127.51, 126.91, 126.24, 125.73, 125.55, 125.33, 125.22, 124.88, 124.77, 121.33, 120.52, 118.35; HRMS (APCI positive) calcd for $C_{52}H_{28}BN_3O_2$ $[M + H]^+$: 738.2334, found 738.2303.

Compound ***5c***. The solution of compound **4c** (0.132 mmol, 100 mg) in DCM (10 mL) was treated with DIPEA (1.32 mmol, 170 mg) and stirred for 10 min at room temperature. Then, the solution of $BF_3{\cdot}Et_2O$ (1.98 mmol, 281 mg) was added dropwise and the mixture was stirred overnight at room temperature. Then, the reaction mixture was slowly quenched with methanol (10 mL) and the resulting precipitate was filtered, yielding 90 mg (85%) of pure dye **5c**. ^{1}H NMR (500 MHz, $CDCl_3$) δ 8.57 (d, $J_{H,H}$ = 9.3 Hz, 2H), 8.25−8.23 (m, 6H), 8.17−8.15 (m, 4H), 8.08 (d, $J_{H,H}$ = 9.3 Hz, 2H), 8.03−7.99 (m, 4H), 7.89−7.85 (m, 4H), 7.10 (d, $J_{H,H}$ = 8.9 Hz, 4H), 3.93 (s, 6H); ^{13}C NMR (75 MHz, $CDCl_3$) δ 162.24, 132.01, 131.67, 131.42, 130.97, 129.86, 129.75, 128.24, 127.94, 127.88, 127.50, 126.16, 125.65, 125.31, 125.10, 124.81, 124.50, 124.32, 123.09, 114.58, 55.64; HRMS (APCI positive) calcd for $C_{54}H_{34}BF_2N_3O_2$ $[M + H]^+$: 806.2771, found 806.2694.

Compound ***5d***. The solution of compound **4d** (0.473 mmol, 336 mg) in DCM (20 mL) was treated with DIPEA (4.73 mmol, 610 mg) and stirred for 10 min at room temperature. Then, the solution of $BF_3{\cdot}Et_2O$ (9.46 mmol, 1.39 g) was added dropwise and the mixture was stirred overnight at room temperature. Then, the reaction mixture was slowly quenched with water (20 mL) and the organic layer was washed with water, dried over Na_2SO_4, and evaporated to dryness. The crude product was purified by column chromatography using chloroform as the solvent, yielding 129 mg (36%) of pure dye **5d**. ^{1}H NMR (300 MHz, $CDCl_3$) δ 8.54−8.51 (m, 4H), 8.21 (d, $J_{H,H}$ = 8.0 Hz, 2H), 8.18−8.15 (m, 4H), 8.10 (d, $J_{H,H}$ = 9.3 Hz, 2H), 8.03−7.98 (m, 4H), 7.89−7.83 (m, 4H), 7.72 (dd, $J_{H,H}$ = 5.0, 0.8 Hz, 2H), 7.39 (s, 2H), 7.37−7.34 (m, 2H); ^{13}C NMR (75 MHz, $CDCl_3$) δ 143.83, 134.35, 133.45, 132.12, 131.78, 131.40, 130.95, 130.11, 129.76, 129.71, 128.33, 128.07, 127.48, 127.43, 126.20, 125.71, 125.52, 125.38, 125.07, 124.77, 124.48, 123.03; HRMS (APCI positive) calcd for $C_{48}H_{26}BF_2N_3S_2$ $[M + H]^+$: 758.1688, found 758.1651.

Compound ***5e***. The solution of compound **4d** (0.109 mmol, 100 mg) in DCM (10 mL) was treated with DIPEA (1.09 mmol, 141 mg) and stirred for 10 min at room temperature under an argon atmosphere. Then, the solution of $BF_3{\cdot}Et_2O$ (2.18 mmol, 312 mg) was added dropwise and the mixture was stirred overnight at room temperature under an argon atmosphere. Then, the reaction mixture was slowly quenched with methanol (10 mL) and the resulting precipitate was filtered, yielding 87 mg (67%) of pure dye **5e**. ^{1}H NMR (500 MHz, $CDCl_3$) δ 8.55 (d, J = 9.3 Hz, 2H), 8.29 (d, J = 8.0 Hz, 2H), 8.17 (d, J = 7.6 Hz, 4H), 8.11 (d, J = 9.3 Hz, 2H), 8.03−7.99 (m, 4H), 7.91−7.88 (m, 4H), 7.14 (s, 2H), 5.51−5.50 (m, 4H), 4.90−4.89 (m, 4H), 4.35 (s, 10H); ^{13}C NMR (75 MHz, $CDCl_3$) δ 131.49, 131.31, 131.03, 129.62, 129.47, 128.38, 127.93, 127.70, 127.59, 126.52, 126.12, 125.75, 125.47, 125.17, 125.12, 124.88, 124.52, 73.84, 71.53; HRMS (APCI positive) calcd for $C_{60}H_{38}BF_2N_3Fe_2$ $[M + H]^+$: 962.1935, found 962.1923.

■ ASSOCIATED CONTENT

Supporting Information

The Supporting Information is available free of charge on the ACS Publications website at DOI: 10.1021/acs.jpcc.8b09504.

Characterization details of target compounds and DFT and TDDFT calculation details (PDF)

Crystallographic data (CIF)

■ AUTHOR INFORMATION

Corresponding Authors

*E-mail: rodion@imr.tohoku.ac.jp (R.V.B.).

*E-mail: blank@umn.edu (D.A.B.).

*E-mail: Viktor.Nemykin@umanitoba.ca (V.N.N.).

ORCID

Christopher J. Ziegler: 0000-0002-0142-5161

David A. Blank: 0000-0003-2582-1537

Victor N. Nemykin: 0000-0003-4345-0848

Notes

The authors declare no competing financial interest.

■ ACKNOWLEDGMENTS

Generous support from the Minnesota Supercomputing Institute, NSERC, CFI, NSF (CHE-1464711), NSF MRI (MRI-1420373 and MRI-0922366), University of Manitoba, and WestGrid Canada to V.N.N. is greatly appreciated. We also wish to thank Prof. Alex Nazarenko for help with the X-ray structure of **5b**·C_{60}. R.V.B. is grateful to the crew of Center for

DOI: 10.1021/acs.jpcc.8b09504
J. Phys. Chem. C 2018, 122, 27893−27916

Computational Materials Science and E-IMR center at the Institute for Materials Research, Tohoku University, for continuous support and also thankful to the Ministry of Education, Culture, Sports, Science, and Technology of Japan (Grant No. 17H03122) for financial support. Generous support from the NSF support (DMR-1708177) to D.A.B. is greatly appreciated.

REFERENCES

(1) D'Souza, F.; Ito, O. In *Handbook of Porphyrin Science*; Kadish, K. M., Smith, K. M., Guilard, R., Eds.; World Scientific Publishing Co. Pte. Ltd., Vol. *1*, pp 307−438.
(2) El-Khouly, M. E.; Ito, O.; Smith, P. M.; D'Souza, F. Intermolecular and Supramolecular Photoinduced Electron Transfer Processes of Fullerene−Porphyrin/Phthalocyanine Systems. *J. Photochem. Photobiol., C* **2004**, *5*, 79−104.
(3) Fukuzumi, S. Development of Bioinspired Artificial Photosynthetic Systems. *Phys. Chem. Chem. Phys.* **2008**, *10*, 2283−2297.
(4) D'Souza, F.; Ito, O. In *Organic Electronics and Photonics*; Nalwa, H. R., Ed.; American Scientific Publishers: Stevenson Ranch, CA, 2008; Chapter 13, Vol. *1*.
(5) Ohkubo, K.; Fukuzumi, S. Rational Design and Functions of Electron Donor−Acceptor Dyads with Much Longer Charge-Separated Lifetimes than Natural Photosynthetic Reaction Centers. *Bull. Chem. Soc. Jpn.* **2009**, *82*, 303−315.
(6) González-Rodríguez, D.; Torres, T.; Guldi, D. M.; Rivera, J.; Herranz, M. A.; Echegoyen, L. Subphthalocyanines: Tuneable Molecular Scaffolds for Intramolecular Electron and Energy Transfer Processes. *J. Am. Chem. Soc.* **2004**, *126*, 6301−6313.
(7) Rudolf, M.; Trukhina, O.; Perles, J.; Feng, L.; Akasaka, T.; Torres, T.; Guldi, D. M. Taming C_{60} Fullerene: Tuning Intramolecular Photoinduced Electron Transfer Process with Subphthalocyanines. *Chem. Sci.* **2015**, *6*, 4141−4147.
(8) González-Rodríguez, D.; Torres, T.; Guldi, D. M.; Rivera, J.; Echegoyen, L. Energy Transfer Processes in Novel Subphthalocyanine−Fullerene Ensembles. *Org. Lett.* **2002**, *4*, 335−338.
(9) Fukuzumi, S. Development of Bioinspired Artificial Photosynthetic Systems. *Phys. Chem. Chem. Phys.* **2008**, *10*, 2283−2297.
(10) Ikemoto, J.; Takimiya, K.; Aso, Y.; Otsubo, T.; Fujitsuka, M.; Ito, O. Porphyrin−Oligothiophene−Fullerene Triads as an Efficient Intramolecular Electron-Transfer System. *Org. Lett.* **2002**, *4*, 309−311.
(11) Gotfredsen, H.; Jevric, M.; Kadziola, A.; Nielsen, M. B. Acetylenic Scaffolding with Subphthalocyanines. *Eur. J. Org. Chem.* **2016**, *2016*, 17−21.
(12) Rahman, G. M. A.; Troeger, A.; Sgobba, V.; Guldi, D. M.; Jux, N.; Balbino, D.; Tchoul, M. N.; Ford, W. T.; Mateo-Alonso, A.; Prato, M. Improving Photocurrent Generation: Supramolecularly and Covalently Functionalized Single-Wall Carbon Nanotubes−Polymer/Porphyrin Donor−Acceptor Nanohybrids. *Chem. − Eur. J.* **2008**, *14*, 8837−8846.
(13) Mochalov, I. A.; Lapshin, A. N.; Nadtochenko, V. A.; Smirnov, V. A.; Goldshleger, N. F. Photochemical Study of the Zinc Cis-3-(4-Imidazolylphenyl)-1-(Pyridin-2-yl)[60] Fullereno [1,2-c] Pyrrolidine-Meso-Tetraphenylporphyrinate Dyad. *Russ. Chem. Bull.* **2006**, *55*, 1598−1604.
(14) Vecchi, A.; Gatto, E.; Floris, B.; Conte, V.; Venanzi, M.; Nemykin, V. N.; Galloni, P. Tetraferrocenylporphyrins as Active Components of Self-Assembled Monolayers on Gold Surface. *Chem. Commun.* **2012**, *48*, 5145−5147.
(15) Imahori, H.; Mori, Y.; Matano, Y. Nanostructured Artificial Photosynthesis. *J. Photochem. Photobiol., C* **2003**, *4*, 51−83.
(16) Imahori, H.; Tamaki, K.; Araki, Y.; Sekiguchi, Y.; Ito, O.; Sakata, Y.; Fukuzumi, S. Stepwise Charge Separation and Charge Recombination in Ferrocene-meso, meso-Linked Porphyrin Dimer−Fullerene Triad. *J. Am. Chem. Soc.* **2002**, *124*, 5165−5174.
(17) D'Souza, F.; Chitta, R.; Gadde, S.; Islam, D.-M. S.; Schumacher, A. L.; Zandler, M. E.; Araki, Y.; Ito, O. Design and Studies on Supramolecular Ferrocene−Porphyrin−Fullerene Constructs for Generating Long-Lived Charge Separated States. *J. Phys. Chem. B* **2006**, *110*, 25240−25250.
(18) Springer, J.; Kodis, G.; De La Garza, L.; Moore, A. L.; Moore, T. A.; Gust, D. Stepwise Sequential and Parallel Photoinduced Charge Separation in a Porphyrin−Triquinone Tetrad. *J. Phys. Chem. A* **2003**, *107*, 3567−3575.
(19) González-Rodríguez, D.; Bottari, G. Phthalocyanines, Subphthalocyanines and Porphyrins for Energy and Electron Transfer Applications. *J. Porphyrins Phthalocyanines* **2009**, *13*, 624−636.
(20) Hochmuth, D. H.; Michel, S. L. J.; White, A. J. P.; Williams, D. J.; Barrett, A. G. M.; Hoffman, B. M. Ci Symmetric and Non-Centrosymmetric Crystalline Complexes of [60] Fullerene with Octakis(Dimethylamino)Porphyrazinato-Copper (II) and-Nickel (II). *Eur. J. Inorg. Chem.* **2000**, 593−596.
(21) Eichhorn, D. M.; Yang, S. L.; Jarrell, W.; Baumann, T. F.; Beall, L. S.; White, A. J. P.; Williams, D. J.; Barreyy, A. G. M.; Hoffman, B. M. [60] Fullerene and TCNQ Donor−Acceptor crystals of Octakis-(Dimethylamino)Porphyrazine. *J. Chem. Soc., Chem. Commun.* **1995**, 1703−1704.
(22) Higashino, T.; Sugiura, K.; Tsuji, Y.; Nimura, S.; Ito, S.; Imahori, H. A Push−Pull Porphyrin Dimer with Multiple Electron-donating Groups for Dye-sensitized Solar Cells: Excellent Light-harvesting in Near-infrared Region. *Chem. Lett.* **2016**, *45*, 1126−1128.
(23) Adineh, M.; Tahay, P.; Huang, W.-K.; Wu, H.-P.; Diau, E. W.-G.; Safari, N. Synthesis of Push−Pull Porphyrin Dyes with Dimethylaminonaphthalene Electron-Donating Groups and their Application to Dye-Sensitized Solar Cells. *RSC Adv.* **2016**, *6*, No. 102979.
(24) Higashino, T.; Kawamoto, K.; Sugiura, K.; Fujimori, Y.; Tsuji, Y.; Kurotobi, K.; Ito, S.; Imahori, H. Effects of Bulky Substituents of Push−Pull Porphyrins on Photovoltaic Properties of Dye-Sensitized Solar Cells. *ACS Appl. Mater. Interfaces* **2016**, *8*, 15379−15390.
(25) Higashino, T.; Fujimori, Y.; Sugiura, K.; Tsuji, Y.; Ito, S.; Imahori, H. Synthesis of Push−Pull Porphyrin with Two Electron-Donating and Two Electron-Withdrawing Groups and its Application to Dye-Sensitized Solar Cell. *J. Porphyrins Phthalocyanines* **2015**, *19*, 140−149.
(26) Ambre, R. B.; Chang, G.-F.; Zanwar, M. R.; Yao, C.-F.; Diau, E. W.-G.; Hung, C.-H. New Dual Donor−Acceptor (2D-π-2A) Porphyrin Sensitizers for Stable and Cost-Effective Dye-Sensitized Solar Cells. *Chem. Asian J.* **2013**, *8*, 2144−2153.
(27) Kang, S. H.; Choi, I. T.; Kang, M. S.; Eom, Y. K.; Ju, M. J.; Hong, J. Y.; Kang, H. S.; Kim, H. K. Novel D−π−A Structured Porphyrin Dyes with Diphenylamine Derived Electron-Donating Substituents for Highly Efficient Dye-Sensitized Solar Cells. *J. Mater. Chem. A* **2013**, *1*, 3977−3982.
(28) Hayashi, H.; Touchy, A. S.; Kinjo, Y.; Kurotobi, K.; Toude, Y.; Ito, S.; Saarenpaeae, H.; Tkachenko, N. V.; Lemmetyinen, H.; Imahori, H. Triarylamine-Substituted Imidazole-and Quinoxaline-Fused Push−Pull Porphyrins for Dye-Sensitized Solar Cells. *ChemSusChem* **2013**, *6*, 508−517.
(29) Mathew, S.; Iijima, H.; Toude, Y.; Umeyama, T.; Matano, Y.; Ito, S.; Tkachenko, N. V.; Lemmetyinen, H.; Imahori, H. Optical, Electrochemical, and Photovoltaic Effects of an Electron-Withdrawing Tetrafluorophenylene Bridge in a Push−Pull Porphyrin Sensitizer Used for Dye-Sensitized Solar Cells. *J. Phys. Chem. C* **2011**, *115*, 14415−14424.
(30) Lo, C.-F.; Hsu, S.-J.; Wang, C.-L.; Cheng, Y.-H.; Lu, H.-P.; Diau, E. W.-G.; Lin, C.-Y. Tuning Spectral and Electrochemical Properties of Porphyrin-Sensitized Solar Cells. *J. Phys. Chem. C* **2010**, *114*, 12018−12023.
(31) Hsieh, C.-P.; Lu, H.-P.; Chiu, C.-L.; Lee, C.-W.; Chuang, S.-H.; Mai, C.-L.; Yen, W.-N.; Hsu, S.-J.; Diau, E. W.-G.; Yeh, C.-Y. Synthesis and Characterization of Porphyrin Sensitizers with Various Electron-Donating Substituents for Highly Efficient Dye-Sensitized Solar Cells. *J. Mater. Chem.* **2010**, *20*, 1127−1134.
(32) Molina, D.; El-Khouly, M. E.; El-Kemary, M.; Fukuzumi, S.; Fernandez-Lazaro, F.; Sastre-Santos, A. Light-Harvesting Phthalocya-

DOI: 10.1021/acs.jpcc.8b09504
J. Phys. Chem. C 2018, 122, 27893−27916

nine−Diketopyrrolopyrrole Derivatives: Synthesis, Spectroscopic, Electrochemical, and Photochemical Studies. *Chem. − Eur. J.* **2016**, *22*, 17800−17807.
(33) Yamamoto, S.; Zhang, A.; Stillman, M. J.; Kobayashi, N.; Kimura, M. Low-Symmetry Ω-Shaped Zinc Phthalocyanine Sensitizers with Panchromatic Light-Harvesting Properties for Dye-Sensitized Solar Cells. *Chem. − Eur. J.* **2016**, *22*, 18760−18768.
(34) El-Khouly, M. E.; Fukuzumi, S. Light Harvesting a Gold Porphyrin−Zinc Phthalocyanine Supramolecular Donor−Acceptor Dyad. *Photochem. Photobiol. Sci.* **2016**, *15*, 1340−1346.
(35) Yang, H.; Pan, S.; Ma, D.; He, D.; Wang, Y.; Xie, S.; Peng, Y. Light-Harvesting Dendrimer Zinc-Phthalocyanines Chromophores Labeled Single-Wall Carbon Nanotube Nanoensembles: Synthesis and Photoinduced Electron Transfer. *J. Lumin.* **2016**, *179*, 588−594.
(36) Yamamoto, S.; Ikeuchi, T.; Mori, S.; Kimura, M. Light-Harvesting in the Near-Infrared Region: Dye-Sensitized Solar Cells Sensitized with Asymmetric Ring-Expanded Zinc (II) Phthalocyanines. *Asian J. Org. Chem.* **2014**, *3*, 1083−1088.
(37) Ikeuchi, T.; Nomoto, H.; Masaki, N.; Griffith, M. J.; Mori, S.; Kimura, M. Molecular Engineering of Zinc Phthalocyanine Sensitizers for Efficient Dye-Sensitized Solar Cells. *Chem. Commun.* **2014**, *50*, 1941−1943.
(38) Vengris, M.; Larsen, D. S.; Valkunas, L.; Kodis, G.; Herrero, C.; Gust, D.; Moore, T.; Moore, A.; van Grondelle, R. Separating Annihilation and Excitation Energy Transfer Dynamics in Light Harvesting Systems. *J. Phys. Chem. B* **2013**, *117*, 11372−11382.
(39) Ishida, Y.; Shimada, T.; Takagi, S. Artificial Light-Harvesting Model in a Self-Assembly Composed of Cationic Dyes and Inorganic Nanosheet. *J. Phys. Chem. C* **2013**, *117*, 9154−9163.
(40) Kimura, M.; Nomoto, H.; Suzuki, H.; Ikeuchi, T.; Matsuzaki, H.; Murakami, T. N.; Furube, A.; Masaki, N.; Griffith, M. J.; Mori, S. Molecular Design Rule of Phthalocyanine Dyes for Highly Efficient Near-IR Performance in Dye-Sensitized Solar Cells. *Chem. − Eur. J.* **2013**, *19*, 7496−7502.
(41) KC, C. B.; Lim, G. N.; D'Souza, F. Tuning Optical and Electron Donor Properties by Peripheral Thio−Aryl Substitution of Subphthalocyanine: A New Series of Donor−Acceptor Hybrids for Photoinduced Charge Separation. *Chem. Asian J.* **2016**, *11*, 1246−1256.
(42) KC, C. B.; Lim, G. N.; Zandler, M. E.; D'Souza, F. Synthesis and Photoinduced Electron Transfer Studies of a Tri-(Phenothiazine)−Subphthalocyanine−Fullerene Pentad. *Org. Lett.* **2013**, *15*, 4612−4615.
(43) Sari, F. A.; Yuzer, A.; Cambarau, W.; Ince, M. Subphthalocyanine Derivatives as Donor for Solution-Processed Small Molecule Organic Solar Cells. *J. Porphyrins Phthalocyanines* **2016**, *20*, 1114−1121.
(44) Weidner, T.; Baio, J. E.; Seibel, J.; Siemeling, U. Dithienylcyclopentene-Functionalised Subphthalocyaninatoboron Complexes: Photochromism, Luminescence Modulation and Formation of Self-Assembled Monolayers on Gold. *Dalton Trans.* **2012**, *41*, 1553−1561.
(45) Sakamoto, K.; Yoshino, S.; Takemoto, M.; Sugaya, K.; Kubo, H.; Komoriya, T.; Kamei, S.; Furukawa, S. Optical and Electrochemical Properties of Non-Peripheral Thioaryl-Substituted Subphthalocyanine as Precursors for Dye-Sensitizer to Develop Photovoltaic Cells. *Am. J. Anal. Chem.* **2014**, *05*, 1037−1045.
(46) Ohno-Okumura, E.; Sakamoto, K.; Kato, T.; Hatano, T.; Fukui, K.; Karatsu, T.; Kitamura, A.; Urano, T. Synthesis of Subphthalocyanine Derivatives and Their Characterization. *Dyes Pigm.* **2002**, *53*, 57−65.
(47) Fernández-Ariza, J.; Calderón, R. M. K.; Perles, J.; Rodríguez-Morgade, M. S.; Guldi, D. M.; Torres, T. Tri- and Hexaferrocenyl-Substituted Subphthalocyanines in the Quest for the Optimum Electron Donor−Acceptor Distances. *Chem. Commun.* **2017**, *53*, 8525−8528.
(48) Jiang, X.-D.; Fang, T.; Liu, X.; Xi, D. Synthesis of Red-Shifted Meso-CF_3-BODIPYs. *Eur. J. Org. Chem.* **2017**, *2017*, 5074−5079.
(49) Yu, C.; Wu, Q.; Wang, J.; Wei, Y.; Hao, E.; Jiao, L. Red to Near-Infrared Isoindole BODIPY Fluorophores: Synthesis, Crystal Structures, and Spectroscopic and Electrochemical Properties. *J. Org. Chem.* **2016**, *81*, 3761−3770.
(50) Zatsikha, Y. V.; Yakubovskyi, V. P.; Shandura, M. P.; Kovtun, Y. P. Boradipyrromethenecyanines on the Base of a BODIPY Nucleus Annelated With a Pyridone Ring: a New Approach to Long-Wavelength Dual Fluorescent Probe Design. *RSC Adv.* **2013**, *3*, 24193−24201.
(51) Martin, A.; Long, C.; Forster, R. J.; Keyes, T. E. Near IR Emitting BODIPY Fluorophores With Mega-Stokes Shifts. *Chem. Commun.* **2012**, *48*, 5617−5619.
(52) Buyukcakir, O.; Bozdemir, O. A.; Kolemen, S.; Erbas, S.; Akkaya, E. U. Tetrastyryl-Bodipy Dyes: Convenient Synthesis and Characterization of Elusive Near IR Fluorophores. *Org. Lett.* **2009**, *11*, 4644−4647.
(53) Qi, X.; Kim, S. K.; Jun, E. J.; Xu, L.; Kim, S.-J.; Yoon, J. A New Bodipy Derivative Bearing Piperazine Group. *Bull. Korean Chem. Soc.* **2007**, *28*, 2231−2234.
(54) Shandura, M. P.; Yakubovskyi, V. P.; Gerasov, A. O.; Kachkovsky, O. D.; Poronik, Y. M.; Kovtun, Y. P. α-Polymethine-Substituted Boron Dipyrromethenes−BODIPY-Based NIR Cyanine-Like Dyes. *Eur. J. Org. Chem.* **2012**, *2012*, 1825−1834.
(55) Adarsh, N.; Krishnan, M. S.; Ramaiah, D. Sensitive Naked Eye Detection of Hydrogen Sulfide and Nitric Oxide by Aza-BODIPY Dyes in Aqueous Medium. *Anal. Chem.* **2014**, *86*, 9335−9342.
(56) Sheng, W.; Cui, J.; Ruan, Z.; Yan, L.; Wu, Q.; Yu, C.; Wei, Y.; Hao, E.; Jiao, L. [a]-Phenanthrene-Fused BF_2 Azadipyrromethene (AzaBODIPY) Dyes as Bright Near-Infrared Fluorophores. *J. Org. Chem.* **2017**, *82*, 10341−10349.
(57) Yamane, H.; Ohtani, S.; Tanaka, K.; Chujo, Y. Synthesis of Furan-Substituted Aza-BODIPYs Having Near-Infrared Emission. *Tetrahedron Lett.* **2017**, *58*, 2989−2992.
(58) Antina, E. V.; Bumagina, N. A. Tetraaryl-Substituted Aza-BODIPY: Synthesis, Spectral Properties, and Possible Applications. *Chem. Heterocycl. Compd.* **2017**, *53*, 39−41.
(59) Shimizu, S.; Iino, T.; Saeki, A.; Seki, S.; Kobayashi, N. Rational Molecular Design towards Vis/NIR Absorption and Fluorescence by using Pyrrolopyrrole aza-BODIPY and its Highly Conjugated Structures for Organic Photovoltaics. *Chem. − Eur. J.* **2015**, *21*, 2893−2904.
(60) Bandi, V.; Gobeze, H. B.; D'Souza, F. Ultrafast Photoinduced Electron Transfer and Charge Stabilization in Donor−Acceptor Dyads Capable of Harvesting Near-Infrared Light. *Chem. − Eur. J.* **2015**, *21*, 11483−11494.
(61) Cidlina, A.; Miletin, M.; Fathi-Rasekh, M.; Nemykin, V. N.; Zimcik, P.; Novakova, V. OFF-ON-OFF Red-Emitting Fluorescent Indicators for a Narrow pH Window. *Chem. − Eur. J.* **2017**, *23*, 1795−1804.
(62) Majeed, S. A.; Ghazal, B.; Nevonen, D. E.; Goff, P. C.; Blank, D. A.; Nemykin, V. N.; Makhseed, S. Evaluation of the Intramolecular Charge-Transfer Properties in Solvatochromic and Electrochromic Zinc Octa (carbazolyl) phthalocyanines. *Inorg. Chem.* **2017**, *56*, 11640−11653.
(63) Maiuri, M.; Snellenburg, J. J.; van Stokkum, I. H. M.; Pillai, S.; WongCarter, K.; Gust, D.; Moore, T. A.; Moore, A. L.; van Grondelle, R.; Cerullo, G.; Polli, D. Ultrafast Energy Transfer and Excited State Coupling in an Artificial Photosynthetic Antenna. *J. Phys. Chem. B* **2013**, *117*, 14183−14190.
(64) de la Torre, G.; Bottari, G.; Sekita, M.; Hausmann, A.; Guldi, D. M.; Torres, T. A Voyage into the Synthesis and Photophysics of Homo- and Heterobinuclear Ensembles of Phthalocyanines and Porphyrins. *Chem. Soc. Rev.* **2013**, *42*, 8049−8105.
(65) Ragoussi, M.-E.; Ince, M.; Torres, T. Recent Advances in Phthalocyanine-Based Sensitizers for Dye-Sensitized Solar Cells. *Eur. J. Org. Chem.* **2013**, *2013*, 6475−6489.
(66) Kloz, M.; Pillai, S.; Kodis, G.; Gust, D.; Moore, T. A.; Moore, A. L.; van Grondelle, R.; Kennis, J. T. M. New Light-Harvesting Roles

DOI: 10.1021/acs.jpcc.8b09504
J. Phys. Chem. C 2018, 122, 27893−27916

of Hot and Forbidden Carotenoid States in Artificial Photosynthetic Constructs. *Chem. Sci.* **2012**, *3*, 2052−2061.
(67) Romero-Nieto, C.; Guilleme, J.; Fernández-Ariza, J.; Rodríguez-Morgade, M. S.; González-Rodríguez, D.; Torres, T.; Guldi, D. M. Ultrafast Photoinduced Processes in Subphthalocyanine Electron Donor−Acceptor Conjugates Linked by a Single B−N Bond. *Org. Lett.* **2012**, *14*, 5656−5659.
(68) Lager, E.; Liu, J.; Aguilar-Aguilar, A.; Tang, B. Z.; Pena-Cabrera, E. Novel Meso-Polyarylamine-BODIPY Hybrids: Synthesis and Study of their Optical Properties. *J. Org. Chem.* **2009**, *74*, 2053−2058.
(69) Verwilst, P.; Kim, H.-R.; Seo, J.; Sohn, N.-W.; Cha, S.-Y.; Kim, Y.; Maeng, S.; Shin, J.-W.; Kwak, J. H.; Kang, C.; Kim, J. S. Rational Design of in Vivo Tau Tangle-Selective Near-Infrared Fluorophores: Expanding the BODIPY Universe. *J. Am. Chem. Soc.* **2017**, *139*, 13393−13403.
(70) Biyiklioglu, Z.; Keles, T. Electrochemical Pesticide Sensors Based on Electropolymerized Metallophthalocyanines. *Inorg. Chim. Acta* **2017**, *466*, 130−138.
(71) Petrushenko, K. B.; Petrushenko, I. K.; Petrova, O. V.; Sobenina, L. N.; Trofimov, B. A. Novel Environment-Sensitive 8-CF_3-BODIPY Dye with 4-(Dimethylamino) Phenyl Group at the 3-Position: Synthesis and Optical Properties. *Dyes Pigm.* **2017**, *136*, 488−495.
(72) Gawale, Y.; Adarsh, N.; Kalva, S. K.; Joseph, J.; Pramanik, M.; Ramaiah, D.; Sekar, N. Carbazole-Linked Near-Infrared Aza-BODIPY Dyes as Triplet Sensitizers and Photoacoustic Contrast Agents for Deep-Tissue Imaging. *Chem. − Eur. J.* **2017**, *23*, 6570−6578.
(73) Zatsikha, Y. V.; Nemez, D. B.; Davis, R. L.; Singh, S.; Herbert, D. E.; King, A. J.; Ziegler, C. J.; Nemykin, V. N. Testing the Limits of the BOPHY Platform: Preparation, Characterization, and Theoretical Modeling of BOPHYs and Organometallic BOPHYs with Electron-Withdrawing Groups at β-Pyrrolic and Bridging Positions. *Chem. − Eur. J.* **2017**, *23*, 14786−14796.
(74) Erickson, N. R.; Holstrom, C. D.; Rhoda, H. M.; Rohde, G. T.; Zatsikha, Y. V.; Galloni, P.; Nemykin, V. N. Tuning Electron-Transfer Properties in 5,10,15,20-Tetra(1′-hexanoylferrocenyl)Porphyrins as Prospective Systems for Quantum Cellular Automata and Platforms for Four-Bit Information Storage. *Inorg. Chem.* **2017**, *56*, 4717−4728.
(75) Didukh, N. O.; Zatsikha, Y. V.; Rohde, G. T.; Blesener, T. S.; Yakubovskyi, V. P.; Kovtun, Y. P.; Nemykin, V. N. NIR Absorbing Diferrocene-Containing Meso-Cyano-BODIPY with a UV-Vis-NIR Spectrum Remarkably Close to that of Magnesium Tetracyanotetraferrocenyltetraazaporphyrin. *Chem. Commun.* **2016**, *52*, 11563−11566.
(76) Maligaspe, E.; Hauwiller, M. R.; Zatsikha, Y. V.; Hinke, J. A.; Solntsev, P. V.; Blank, D. A.; Nemykin, V. N. Redox and Photoinduced Electron-Transfer Properties in Short Distance Organoboryl Ferrocene-Subphthalocyanine Dyads. *Inorg. Chem.* **2014**, *53*, 9336−9347.
(77) Solntsev, P. V.; Spurgin, K. L.; Sabin, J. R.; Heikal, A. A.; Nemykin, V. N. Photoinduced Charge Transfer in Short-Distance Ferrocenylsubphthalocyanine Dyads. *Inorg. Chem.* **2012**, *51*, 6537−6547.
(78) Solntsev, P. V.; Sabin, J. R.; Dammer, S. J.; Gerasimchuk, N. N.; Nemykin, V. N. Unexpected Fluorescence Properties in an Axially σ-Bonded Ferrocenyl-Containing Porphyrin. *Chem. Commun.* **2010**, *46*, 6581−6583.
(79) Nemykin, V. N.; Rohde, G. T.; Barrett, C. D.; Hadt, R. G.; Bizzarri, C.; Galloni, P.; Floris, B.; Nowik, I.; Herber, R. H.; Marrani, A. G.; Zanoni, R.; Loim, N. M. Electron-Transfer Processes in Metal-Free Tetraferrocenylporphyrin. Understanding Internal Interactions to Access Mixed-Valence States Potentially Useful for Quantum Cellular Automata. *J. Am. Chem. Soc.* **2009**, *131*, 14969−14978.
(80) Burrell, A. K.; Campbell, W. M.; Jameson, G. B.; Officer, D. L.; Boyd, P. D. W.; Zhao, Z.; Cocks, P. A.; Gordon, K. C. Bis(ferrocenyl)Porphyrins. Compounds with Strong Long-Range Metal−Metal Coupling. *Chem. Commun.* **1999**, 637−638.
(81) Galloni, P.; Floris, B.; De Cola, L.; Cecchetto, E.; Williams, R. M. Zinc 5,10,15,20-Meso-Tetraferrocenylporphyrin as an Efficient Donor in a Supramolecular Fullerene C_{60} System. *J. Phys. Chem. C* **2007**, *111*, 1517−1523.
(82) Jin, Z.; Nolan, K.; McArthur, C. R.; Lever, A. B. P.; Leznoff, C. C. Synthesis, Electrochemical and Spectroelectrochemical Studies of Metal-Free 2,9,16,23-Tetraferrocenylphthalocyanine. *J. Organomet. Chem.* **1994**, *468*, 205−212.
(83) Pomarico, G.; Vecchi, A.; Mandoj, F.; Bortolini, O.; Cicero, D. O.; Galloni, P.; Paolesse, R. The Corrole and Ferrocene Marriage: 5,10,15-Triferrocenylcorrolato Cu. *Chem. Commun.* **2014**, *50*, 4076−4978.
(84) Galangau, O.; Fabre-Francke, I.; Munteanu, S.; Dumas-Verdes, C.; Clavier, G.; Meallet-Renault, R.; Pansu, R. B.; Hartl, F.; Miomandre, F. Electrochromic and Electrofluorochromic Properties of a New Boron Dipyrromethene−Ferrocene Conjugate. *Electrochim. Acta* **2013**, *87*, 809−815.
(85) Misra, R.; Dhokale, B.; Jadhav, T.; Mobin, S. M. Donor−Acceptor Meso-Alkynylated Ferrocenyl BODIPYs: Synthesis, Structure, and Properties. *Dalton Trans.* **2013**, *42*, 13658−13666.
(86) Yin, X.; Li, Y.; Li, Y.; Zhu, Y.; Tang, X.; Zheng, H.; Zhu, D. Electrochromism Based on the Charge Transfer Process in a Ferrocene−BODIPY Molecule. *Tetrahedron* **2009**, *65*, 8373−8377.
(87) Misra, R.; Dhokale, B.; Jadhav, T.; Mobin, S. M. Heteroatom-Connected Ferrocenyl BODIPYs: Synthesis, Structure, and Properties. *Organometallics* **2014**, *33*, 1867−1877.
(88) Yin, X.; Li, Y.; Zhu, Y.; Jing, X.; Li, Y.; Zhu, D. A Highly Sensitive Viscosity Probe Based on Ferrocene-BODIPY Dyads. *Dalton Trans.* **2010**, *39*, 9929−9935.
(89) Aratani, N.; Osuka, A. In *Handbook of Porphyrin Science*; Kadish, K. M., Smith, K. M., Guilard, R., Eds.; World Scientific Publishing Co. Pte. Ltd., 2010; Vol. *1*, pp 1−132.
(90) Balaban, T. S. In *Handbook of Porphyrin Science*; Kadish, K. M., Smith, K. M., Guilard, R., Eds.; World Scientific Publishing Co. Pte. Ltd., 2010; Vol. *1*, pp 221−306.
(91) Verreet, B.; Rand, B. P.; Cheyns, D.; Hadipour, A.; Aernouts, T.; Heremans, P.; Medina, A.; Claessens, C. G.; Torres, T. A 4% Efficient Organic Solar Cell Using a Fluorinated Fused Subphthalocyanine Dimer as an Electron Acceptor. *Adv. Energy Mater.* **2011**, *1*, 565−568.
(92) Luhman, W. A.; Holmes, R. J. Investigation of Energy Transfer in Organic Photovoltaic Cells and Impact on Exciton Diffusion Length Measurements. *Adv. Funct. Mater.* **2011**, *21*, 764−771.
(93) Della Pia, A.; Riello, M.; Stassen, D.; Jones, T. S.; Bonifazi, D.; De Vita, A.; Costantini, G. Two-Dimensional Core−Shell Donor−Acceptor Assemblies at Metal−Organic Interfaces Promoted by Surface-Mediated Charge Transfer. *Nanoscale* **2016**, *8*, 19004−19013.
(94) Saito, K.; Kashiwagi, Y.; Ohkubo, K.; Fukuzumi, S. An Extremely Long-Lived Charge-Separated State of Zinc Tetraphenylporphyrin Coordinated with Pyridylnaphthalene-Diimide. *J. Porphyrins Phthalocyanines* **2006**, *10*, 1371−1379.
(95) Vecchi, A.; Erickson, N. R.; Sabin, J. R.; Floris, B.; Conte, V.; Venanzi, M.; Galloni, P.; Nemykin, V. N. Electronic Properties of Mono-Substituted Tetraferrocenyl Porphyrins in Solution and on a Gold Surface: Assessment of the Influencing Factors for Photoelectrochemical Applications. *Chem. − Eur. J.* **2015**, *21*, 269−279.
(96) KC, C. B.; D'Souza, F. Design and Photochemical Study of Supramolecular Donor−Acceptor Systems Assembled via Metal−Ligand Axial Coordination. *Coord. Chem. Rev.* **2016**, *322*, 104−141.
(97) Krishna, V. S. R.; Samanta, M.; Pal, S.; Anurag, N. P.; Bandyopadhyay, S. Light-Triggered Assembly−Disassembly of an Ordered Donor−Acceptor π-Stack Using a Photoresponsive Dimethyldihydropyrene π-Switch. *Org. Biomol. Chem.* **2016**, *14*, 5744−5750.
(98) Xu, Z.; Gao, F.; Makarova, E. A.; Heikal, A. A.; Nemykin, V. N. Energy Transfer from Colloidal Quantum Dots to Near-Infrared-Absorbing Tetraazaporphyrins for Enhanced Light Harvesting. *J. Phys. Chem. C* **2015**, *119*, 9754−9761.

DOI: 10.1021/acs.jpcc.8b09504
J. Phys. Chem. C 2018, 122, 27893−27916

(99) Gust, D. Supramolecular Photochemistry Applied to Artificial Photosynthesis and Molecular Logic Devices. *Faraday Discuss.* **2015**, *185*, 9−35.
(100) Guo, J.; Liang, Y.; Xiao, S.; Szarko, J. M.; Sprung, M.; Mukhopadhyay, M. K.; Wang, J.; Yu, L.; Chen, L. X. Structure and Dynamics Correlations of Photoinduced Charge Separation in Rigid Conjugated Linear Donor−Acceptor Dyads towards Photovoltaic Applications. *New J. Chem.* **2009**, *33*, 1497−1507.
(101) Das, A.; Ghosh, S. Supramolecular Assemblies by Charge-Transfer Interactions between Donor and Acceptor Chromophores. *Angew. Chem., Int. Ed.* **2014**, *53*, 2038−2054.
(102) Dammer, S. J.; Solntsev, P. V.; Sabin, J. R.; Nemykin, V. N. Synthesis, Characterization, and Electron-Transfer Processes in Indium Ferrocenyl-Containing Porphyrins and their Fullerene Adducts. *Inorg. Chem.* **2013**, *52*, 9496−9510.
(103) Scarel, F.; Ehli, C.; Guldi, D. M.; Mateo-Alonso, A. A Non-Covalent Strategy to Prepare Electron Donor−Acceptor Rotaxanes. *Chem. Commun.* **2013**, *49*, 9452−9454.
(104) Ince, M.; Hausmann, A.; Martinez-Diaz, M. V.; Guldi, D. M.; Torres, T. Non-Covalent versus Covalent Donor−Acceptor Systems Based on Near-Infrared Absorbing Azulenocyanines and C_{60} Fullerene Derivatives. *Chem. Commun.* **2012**, *48*, 4058−4060.
(105) Amelia, M.; Credi, A. Photosensitization of the Luminescence of CdTe Nanocrystals by Noncovalently Bound Zn Tetraphenylporphyrin. *Inorg. Chim. Acta* **2012**, *381*, 247−250.
(106) Linton, D.; Driva, P.; Sumpter, B.; Ivanov, I.; Geohegan, D.; Feigerle, C.; Dadmun, M. D. The Importance of Chain Connectivity in the Formation of Non-Covalent Interactions between Polymers and Single-Walled Carbon Nanotubes and its Impact on Dispersion. *Soft Matter* **2010**, *6*, 2801−2814.
(107) Sun, B.; Ou, Z.; Meng, D.; Fang, Y.; Song, Y.; Zhu, W.; Solntsev, P. V.; Nemykin, V. N.; Kadish, K. M. Electrochemistry and Catalytic Properties for Dioxygen Reduction Using Ferrocene-Substituted Cobalt Porphyrins. *Inorg. Chem.* **2014**, *53*, 8600−8609.
(108) Rao, M. R.; Sun, S.-S. Supramolecular Assemblies of Amide-Derived Organogels Featuring Rigid π-Conjugated Phenylethynyl Frameworks. *Langmuir* **2013**, *29*, 15146−15158.
(109) Jalani, K.; Kumar, M.; George, S. J. Mixed Donor−Acceptor Charge-Transfer Stacks Formed via Hierarchical Self-Assembly of a Non-Covalent Amphiphilic Foldamer. *Chem. Commun.* **2013**, *49*, 5174−5176.
(110) Ghosh, A.; Rao, K. V.; Voggu, R.; George, S. J. Non-Covalent Functionalization, Solubilization of Graphene and Single-walled Carbon Nanotubes with Aromatic Donor and Acceptor Molecules. *Chem. Phys. Lett.* **2010**, *488*, 198−201.
(111) Pérez, E. M.; Illescas, B. M.; Herranz, M. A.; Martín, N. Supramolecular Chemistry of π-Extended Analogues of TTF and Carbon Nanostructures. *New J. Chem.* **2009**, *33*, 228−234.
(112) Dirian, K.; Herranz, M. A.; Katsukis, G.; Malig, J.; Rodriguez-Perez, L.; Romero-Nieto, C.; Strauss, V.; Martin, N.; Guldi, D. M. Low Dimensional Nanocarbons−Chemistry and Energy/Electron Transfer Reactions. *Chem. Sci.* **2013**, *4*, 4335−4353.
(113) Shen, Y.; Reparaz, J. S.; Wagner, M. R.; Hoffmann, A.; Thomsen, C.; Lee, J.-O.; Heeg, S.; Hatting, B.; Reich, S.; Saeki, A.; et al. Assembly of Carbon Nanotubes and Alkylated Fullerenes: Nanocarbon Hybrid Towards Photovoltaic Applications. *Chem. Sci.* **2011**, *2*, 2243−2250.
(114) Seitz, W.; Kahnt, A.; Guldi, D. M.; Torres, T. Controlling Charge Transfer in Fullerene/Phthalocyanine Electron Donor-Acceptor Conjugates/Hybrids. *J. Porphyrins Phthalocyanines* **2009**, *13*, 1034−1039.
(115) Sandanayaka, A. S. D.; Ito, O. Photoinduced Electron Transfer in Supramolecules Composed of Porphyrin/Phthalocyanine and Nanocarbon Materials. *J. Porphyrins Phthalocyanines* **2009**, *13*, 1017−1033.
(116) Zannotti, M.; Giovannetti, R.; D'Amato, C. A.; Rommozzi, E. Spectroscopic Studies of Porphyrin Functionalized Multiwalled Carbon Nanotubes and their Interaction with TiO_2 Nanoparticles Surface. *Spectrochim. Acta, Part A* **2016**, *153*, 22−29.
(117) Schuster, D. I.; Megiatto, J. D., Jr. Carbon Nanotubes: Nanotubes Reveal all in Solution. *Nat. Chem.* **2009**, *1*, 182−183.
(118) Sandanayaka, A. S. D.; Subbaiyan, N. K.; Das, S. K.; Chitta, R.; Maligaspe, E.; Hasobe, T.; Ito, O.; D'Souza, F. Diameter-Sorted SWCNT−Porphyrin and SWCNT−Phthalocyanine Conjugates for Light-Energy Harvesting. *ChemPhysChem* **2011**, *12*, 2266−2273.
(119) Bartelmess, J.; Soares, A. R. M.; Martinez-Diaz, M. V.; Neves, M. G. P. M. S.; Tome, A. C.; Cavaleiro, J. A. S.; Torres, T.; Guldi, D. M. Panchromatic Light Harvesting in Single Wall Carbon Nanotube Hybrids—Immobilization of Porphyrin−Phthalocyanine Conjugates. *Chem. Commun.* **2011**, *47*, 3490−3492.
(120) Ragoussi, M.-E.; Malig, J.; Katsukis, G.; Butz, B.; Spiecker, E.; de la Torre, G.; Torres, T.; Guldi, D. M. Linking Photo-and Redoxactive Phthalocyanines Covalently to Graphene. *Angew. Chem., Int. Ed.* **2012**, *51*, 6421−6425.
(121) Bottari, G.; de la Torre, G.; Guldi, D. M.; Torres, T. Covalent and Noncovalent Phthalocyanine−Carbon Nanostructure Systems: Synthesis, Photoinduced Electron Transfer, and Application to Molecular Photovoltaics. *Chem. Rev.* **2010**, *110*, 6768−6816.
(122) Li, Y.; Rhoda, H. M.; Wertish, A. M.; Nemykin, V. N. Organometallic Pyrene-Containing Porphyrins: Synthesis, Characterization, and Non-Covalent Interactions with C_{60} Fullerenes. *J. Porphyrins Phthalocyanines* **2016**, *20*, 1098−1113.
(123) Nakano, S.; Kage, Y.; Furuta, H.; Kobayashi, N.; Shimizu, S. Pyrene-Bridged Boron Subphthalocyanine Dimers: Combination of Planar and Bowl-Shaped π-Conjugated Systems for Creating Uniquely Curved π-Conjugated Systems. *Chem. − Eur. J.* **2016**, *22*, 7706−7710.
(124) KC, C. B.; Lim, G. N.; D'Souza, F. Charge Separation in Graphene-Decorated Multimodular Tris (pyrene)−Subphthalocyanine−Fullerene Donor−Acceptor Hybrids. *Angew. Chem., Int. Ed.* **2015**, *54*, 5088−5092.
(125) Ji, L.; Wu, Y.; Ma, L.; Yang, X. Noncovalent Functionalization of Graphene with Pyrene-Terminated Liquid Crystalline Polymer. *Composites, Part A* **2015**, *72*, 32−39.
(126) Hayes, W.; Greenland, B. W. Donor−Acceptor π−π Stacking Interactions: From Small Molecule Complexes to Healable Supramolecular Polymer Networks. *Adv. Polym. Sci.* **2015**, *268*, 143−166.
(127) Umeyama, T.; Baek, J.; Mihara, J.; Tkachenko, N. V.; Imahori, H. Occurrence of Photoinduced Charge Separation by the Modulation of the Electronic Coupling between Pyrene Dimers and Chemically Converted Graphenes. *Chem. Commun.* **2017**, *53*, 1025−1028.
(128) Didier, D.; Schulz, E. π-Stacking Interactions at the Service of [Cu]-Bis(Oxazoline) Recycling. *Tetrahedron: Asymmetry* **2013**, *24*, 769−775.
(129) Jameson, L. P.; Dzyuba, S. V. Aza-BODIPY: Improved Synthesis and Interaction with Soluble Aβ1−42 Oligomers. *Bioorg. Med. Chem. Lett.* **2013**, *23*, 1732−1735.
(130) Klfout, H.; Stewart, A.; Elkhalifa, M.; He, H. BODIPYs for Dye-Sensitized Solar Cells. *ACS Appl. Mater. Interfaces* **2017**, *9*, 39873−39889.
(131) Jiang, X.-D.; Li, S.; Guan, J.; Fang, T.; Liu, X.; Xiao, L.-J. Recent Advances of the Near-infrared Fluorescent aza-BODIPY Dyes. *Curr. Org. Chem.* **2016**, *20*, 1736−1744.
(132) Ziegler, C. J.; Chanawanno, K.; Hasheminsasab, A.; Zatsikha, Y. V.; Maligaspe, E.; Nemykin, V. N. Synthesis, Redox Properties, and Electronic Coupling in the Diferrocene Aza-dipyrromethene and azaBODIPY Donor−Acceptor Dyad with Direct Ferrocene−α-Pyrrole Bond. *Inorg. Chem.* **2014**, *53*, 4751−4755.
(133) Nemykin, V. N.; Blesener, T. S.; Ziegler, C. J. Photophysics, Redox Processes, and Electronic Structures of Ferrocenyl-Containing BODIPYs, aza-BODIPYs, BOPHYs, Transition-Metal Dipyrromethenes and aza-Dipyrromethenes. *Macroheterocycles* **2017**, *10*, 9−26.
(134) Vecchi, A.; Galloni, P.; Floris, B.; Nemykin, V. N. New Developments in Chemistry of Organometallic Porphyrins and their Analogs. *J. Porphyrins Phthalocyanines* **2013**, *17*, 165−196.
(135) Ladomenou, K.; Nikolaou, V.; Charalambidis, G.; Charisiadis, A.; Coutsolelos, A. G. Porphyrin−BODIPY-Based Hybrid Model

DOI: 10.1021/acs.jpcc.8b09504
J. Phys. Chem. C 2018, 122, 27893−27916

Compounds for Artificial Photosynthetic Reaction Centers. *C. R. Chim.* **2017**, *20*, 314−322.
(136) Singh, S. P.; Gayathri, T. Evolution of BODIPY Dyes as Potential Sensitizers for Dye-Sensitized Solar Cells. *Eur. J. Org. Chem.* **2014**, *2014*, 4689−4707.
(137) Arbeloa, F. L.; Banuelos, J.; Martinez, V.; Arbeloa, T.; Arbeloa, I. L. A General Overview on the Photophysics of BODIPY Dyes in Liquid Solutions and Solid Polymer Matrices. *Trends Phys. Chem.* **2008**, *13*, 101−122.
(138) Zatsikha, Y. V.; Didukh, N. O.; Nemez, D.; Schlachter, A. C.; Karsenti, P.-L.; Kovtun, Y. P.; Harvey, P. D.; Nemykin, V. N. Ferrocene−BODIPYmerocyanine Dyads: New NIR Absorbing Platforms with Optical Properties Susceptible to Protonation. *Chem. Commun.* **2017**, *53*, 7612−7615.
(139) Zatsikha, Y. V.; Didukh, N. O.; Blesener, T.; Kayser, M. P.; Kovtun, Y. P.; Blank, D. A.; Nemykin, V. N. Preparation, Characterization, Redox, and Photoinduced Electron-Transfer Properties of the NIR-Absorbing N-Ferrocenyl-2-pyridone BODIPYs. *Eur. J. Inorg. Chem.* **2017**, *2017*, 318−324.
(140) Maligaspe, E.; Pundsack, T. J.; Albert, L. M.; Zatsikha, Y. V.; Solntsev, P. V.; Blank, D. A.; Nemykin, V. N. Synthesis and Charge-Transfer Dynamics in a Ferrocene-Containing Organoboryl Aza-BODIPY Donor−Acceptor Triad with Boron as the Hub. *Inorg. Chem.* **2015**, *54*, 4167−4174.
(141) Rhoda, H. M.; Chanawanno, K.; King, A. J.; Zatsikha, Y. V.; Ziegler, C. J.; Nemykin, V. N. Unusually Strong Long-Distance Metal−Metal Coupling in Bis(Ferrocene)-Containing BOPHY: An Introduction to Organometallic BOPHYs. *Chem. − Eur. J.* **2015**, *21*, 18043−18046.
(142) Filatov, M. A.; Karuthedath, S.; Polestshuk, P. M.; Savoie, H.; Flanagan, K. J.; Sy, C.; Sitte, E.; Telitchko, M.; Laquai, F.; Boyle, R. W.; Senge, M. O. Generation of Triplet Excited States via Photoinduced Electron Transfer in Meso-Anthra-BODIPY: Fluorogenic Response toward Singlet Oxygen in Solution and in Vitro. *J. Am. Chem. Soc.* **2017**, *139*, 6282−6285.
(143) Zhao, J.; Xu, K.; Yang, W.; Wang, Z.; Zhong, F. The Triplet Excited State of Bodipy: Formation, Modulation and Application. *Chem. Soc. Rev.* **2015**, *44*, 8904−8939.
(144) Zatsikha, Y. V.; Maligaspe, E.; Purchel, A. A.; Didukh, N. O.; Wang, Y.; Kovtun, Y. P.; Blank, D. A.; Nemykin, V. N. Tuning Electronic Structure, Redox, and Photophysical Properties in Asymmetric NIR-Absorbing Organometallic BODIPYs. *Inorg. Chem.* **2015**, *54*, 7915−7928.
(145) Boens, N.; Leen, V.; Dehaen, W. Fluorescent Indicators Based on BODIPY. *Chem. Soc. Rev.* **2012**, *41*, 1130−1172.
(146) Vecchi, A.; Galloni, P.; Floris, B.; Dudkin, S. V.; Nemykin, V. N. Metallocenes Meet Porphyrinoids: Consequences of a "Fusion. *Coord. Chem. Rev.* **2015**, *291*, 95−171.
(147) Zatsikha, Y. V.; Holstrom, C. D.; Chanawanno, K.; Osinski, A. J.; Ziegler, C. J.; Nemykin, V. N. Observation of the Strong Electronic Coupling in Near-Infrared-Absorbing Tetraferrocene aza-Dipyrromethene and aza-BODIPY with Direct Ferrocene−α-and Ferrocene−β-Pyrrole Bonds: Toward Molecular Machinery with Four-Bit Information Storage Capacity. *Inorg. Chem.* **2017**, *56*, 991−1000.
(148) Robin, M. B.; Day, P. *Advances Inorganic Chemistry and Radiochemistry*; Academic Press: New York, 1967; Vol. *10*, pp 247−422.
(149) Hush, N. S. Intervalence-Transfer Absorption. Part 2. Theoretical Considerations and Spectroscopic Data. *Prog. Inorg. Chem.* **2007**, *8*, 391−444.
(150) Hush, N. S. Distance Dependence of Electron Transfer Rates. *Coord. Chem. Rev.* **1985**, *64*, 135−157.
(151) Feltham, H. L. C.; Dankhoff, K.; Meledandri, C. J.; Brooker, S. Towards Dual-Functionality Spin-Crossover Complexes. *ChemPlusChem* **2018**, 582−589.
(152) Zhang, Y.; Ma, R.; Zhen, X. V.; Kudva, Y. C.; Buhlmann, P.; Koester, S. Capacitive Sensing of Glucose in Electrolytes Using Graphene Quantum Capacitance Varactors. *ACS Appl. Mater. Interfaces* **2017**, *9*, 38863−38869.
(153) Zhang, X.; Jia, C.; Xue, Y. Fabrication of CdTe QD-rGO Composites with Different Linkers for Controlling Charge Separation and Recombination. *Mater. Res. Bull.* **2018**, *98*, 53−58.
(154) Zaharie-Butucel, D.; Potara, M.; Craciun, A. M.; Boukherroub, R.; Szunerits, S.; Astilean, S. Revealing the Structure and Functionality of Graphene Oxide and Reduced Graphene Oxide/Pyrene Carboxylic Acid Interfaces by Correlative Spectral and Imaging Analysis. *Phys. Chem. Chem. Phys.* **2017**, *19*, 16038−16046.
(155) Hinnemo, M.; Zhao, J.; Ahlberg, P.; Haegglund, C.; Djurberg, V.; Scheicher, R. H.; Zhang, S.-L.; Zhang, Z.-B. On Monolayer Formation of Pyrenebutyric Acid on Graphene. *Langmuir* **2017**, *33*, 3588−3593.
(156) De Filpo, G.; Nicoletta, F. P.; Ciliberti, L.; Formoso, P.; Chidichimo, G. Non-Covalent Functionalisation of Single Wall Carbon Nanotubes for Efficient Dye-Sensitised Solar Cells. *J. Power Sources* **2015**, *274*, 274−279.
(157) Bosch-Navarro, C.; Matt, B.; Izzet, G.; Romero-Nieto, C.; Dirian, K.; Raya, A.; Molina, S. I.; Proust, A.; Guldi, D. M.; Marti-Gastaldo, C.; Coronado, E. Charge Transfer Interactions in Self-Assembled Single Walled Carbon Nanotubes/Dawson−Wells Polyoxometalate Hybrids. *Chem. Sci.* **2014**, *5*, 4346−4354.
(158) Apartsin, E. K.; Buyanova, M. Y.; Novopashina, D. S.; Ryabchikova, E. I.; Filatov, A. V.; Zenkova, M. A.; Venyaminova, A. G. Novel Multifunctional Hybrids of Single-Walled Carbon Nanotubes with Nucleic Acids: Synthesis and Interactions with Living Cells. *ACS Appl. Mater. Interfaces* **2014**, *6*, 1454−1461.
(159) Oevering, H.; Paddon-Row, M. N.; Heppener, M.; Oliver, A. M.; Cotsaris, E.; Verhoeven, J. W.; Hush, N. S. Long-Range Photoinduced Through-Bond Electron Transfer and Radiative Recombination via Rigid Nonconjugated Bridges: Distance and Solvent Dependence. *J. Am. Chem. Soc.* **1987**, *109*, 3258−3269.
(160) Weller, A. Photoinduced Electron Transfer in Solution: Exciplex and Radical Ion Pair Formation Free Enthalpies and their Solvent Dependence. *Z. Phys. Chem.* **1982**, *133*, 93−98.
(161) Rehm, D.; Weller, A. Kinetics of Fluorescence Quenching by Electron and H-Atom Transfer. *Isr. J. Chem.* **1970**, *8*, 259−271.
(162) Kroon, J.; Verhoeven, J. W.; Paddon-row, M. N.; Oliver, A. M. Solvent Dependence of Photoinduced Intramolecular Electron Transfer: Criteria for the Design of Systems with Rapid, Solvent-Independent Charge Separation. *Angew. Chem., Int. Ed.* **1991**, *30*, 1358−1361.
(163) ΔG_{ET} was estimated by the following formula: Where $E^0(D^{+\bullet}/D)$ and $E^0(A/A^{-\bullet})$ are oxidation potential of a donor and reduction potential of an acceptor, respectively; E_{00} excitation energy at the BODIPY; R_{DA} is a donor-accepted distance estimated on a basis of DFT calculations and X-ray data available for non-covalent complexes formed between aza-BODIPYs and C_{60}; ε_s and ε_{EC} are the dielectric constants of the solvents used in photochemical and electrochemical studies; r^+ and r^- are the effective ionic radii of the donor and acceptor, respectively, that are estimated on the basis of DFT calculations.
(164) Zheng, M.; Bai, F.; Li, F.; Li, Y.; Zhu, D. The Interaction Between Conjugated Polymer and Fullerenes. *J. Appl. Polym. Sci.* **1998**, *70*, 599−603.
(165) Rhoda, H. M.; Kayser, M. P.; Wang, Y.; Nazarenko, A. Y.; Belosludov, R. V.; Kiprof, P.; Blank, D. A.; Nemykin, V. N. Tuning up an Electronic Structure of the Subphthalocyanine Derivatives toward Electron-Transfer Process in Noncovalent Complexes with C_{60} and C_{70} Fullerenes: Experimental and Theoretical Studies. *Inorg. Chem.* **2016**, *55*, 9549−9563.
(166) Konarev, D. V.; Troyanov, S. I.; Lyubovskaya, R. N. Coordination Complex of Boron Subphthalocyanine (BSubPc) with Fluorenone Pinacolate: Effective $\pi-\pi$ Interaction of Concave BSubPc Macrocycle with Fullerene C_{60}. *CrystEngComm* **2015**, *17*, 3923−3926.
(167) Sanchez Molina, I.; Ince, M.; Bottari, G.; Claessens, C. G.; Martinez-Diaz, M. V.; Torres, T. Encapsulation of Phthalocyanine-C_{60} Fullerene Conjugates into Metallosupramolecular Subphthalocyanine Capsules: A Turn of the Screw. *Turk. J. Chem.* **2014**, *38*, 1006−1012.

DOI: 10.1021/acs.jpcc.8b09504
J. Phys. Chem. C 2018, 122, 27893−27916

(168) Ke, X.-S.; Kim, T.; Lynch, V. M.; Kim, D.; Sessler, J. L. Flattened Calixarene-like Cyclic BODIPY Array: A New Photosynthetic Antenna Model. *J. Am. Chem. Soc.* **2017**, *139*, 13950−13956.
(169) González-Godríguez, D.; Carbonell, E.; Guldi, D. M.; Torres, T. Modulating Electronic Interactions between Closely Spaced Complementary π Surfaces with Different Outcomes: Regio-and Diastereomerically Pure Subphthalocyanine−C60 Tris Adducts. *Angew. Chem., Int. Ed.* **2009**, *48*, 8032.
(170) Sánchez-Molina, I.; Grimm, B.; Calderon, R. M. K.; Claessens, C. G.; Guldi, D. M.; Torres, T. Self-Assembly, Host−Guest Chemistry, and Photophysical Properties of Subphthalocyanine-Based Metallosupramolecular Capsules. *J. Am. Chem. Soc.* **2013**, *135*, 10503−10511.
(171) González-Rodríguez, D.; Carbonell, E.; de Miguel Rojas, G.; Castellanos, C. A.; Guldi, D. M.; Torres, T. Activating Multistep Charge-Transfer Processes in Fullerene−Subphthalocyanine−Ferrocene Molecular Hybrids as a Function of π−π Orbital Overlap. *J. Am. Chem. Soc.* **2010**, *132*, 16488−16500.
(172) Cantu, R.; Gobeze, H. B.; D'Souza, F. Synthesis and Photochemical Studies of a Tris(4-Iodophenoxy)-Subphthalocyaninato Boron(III)-Fulleropyrrolidine Dyad. *J. Porphyrins Phthalocyanines* **2016**, *20*, 987−996.
(173) KC, C. B.; Lim, G. N.; D'Souza, F. Tuning Optical and Electron Donor Properties by Peripheral Thio−Aryl Substitution of Subphthalocyanine: A New Series of Donor−Acceptor Hybrids for Photoinduced Charge Separation. *Chem. − Eur. J.* **2016**, *22*, 13301−13311.
(174) Mutolo, K. L.; Mayo, E. I.; Rand, B. P.; Forrest, S. R.; Thompson, M. E. Enhanced Open-Circuit Voltage in Subphthalocyanine/C_{60} Organic Photovoltaic Cells. *J. Am. Chem. Soc.* **2006**, *128*, 8108−8109.
(175) Ma, Z.; Liu, S.; Hu, S.; Yu, J. Highly Efficient Tandem Organic Light-Emitting Diodes Based on SubPc:C_{60} Bulk Heterojunction as Charge Generation Layer. *J. Lumin.* **2016**, *169*, 29−34.
(176) Morris, S. E.; Shtein, M. High Efficiency Organic Photovoltaic Cells Based on Inverted SubPc/C_{60}/ITO Cascade Junctions. *Org. Electron.* **2014**, *15*, 3795−3799.
(177) Credgington, D.; Liu, S.-W.; Nelson, J.; Durrant, J. R. In Situ Measurement of Energy Level Shifts and Recombination Rates in Subphthalocyanine/C_{60} Bilayer Solar Cells. *J. Phys. Chem. C* **2014**, *118*, 22858−22864.
(178) Su, W.-C.; Lee, C.-C.; Liu, S.-W.; Lin, C.-F.; Chou, C.-C.; Huang, B.-Y.; Cheng, C.-W. Improving the Performance of Subphthalocyanine/C_{60} Planar Heterojunction Organic Photovoltaic Device Through the Insertion of Molybdenum Oxide Anodic Buffer. *Jpn. J. Appl. Phys.* **2014**, *53*, No. 03CE02.
(179) Kim, J. Y.; Kwak, J.; Noh, S.; Lee, C. Enhanced Performance of SubPC/C_{60} Solar Cells by Annealing and Modifying Surface Morphology. *J. Nanosci. Nanotechnol.* **2012**, *12*, 5724−5727.
(180) Josey, D. S.; Nyikos, S. R.; Garner, R. K.; Dovijarski, A.; Castrucci, J. S.; Wang, J. M.; Evans, G. J.; Bender, T. P. Outdoor Performance and Stability of Boron Subphthalocyanines Applied as Electron Acceptors in Fullerene-Free Organic Photovoltaics. *ACS Energy Lett.* **2017**, *2*, 726−732.
(181) Duan, C.; Zango, G.; Iglesias, M. G.; Colberts, F. J. M.; Wienk, M. M.; Martinez-Diaz, M. V.; Janssen, R. A. J.; Torres, T. The Role of the Axial Substituent in Subphthalocyanine Acceptors for Bulk-Heterojunction Solar Cells. *Angew. Chem., Int. Ed.* **2017**, *56*, 148−152.
(182) Castrucci, J. S.; Josey, D. S.; Thibau, E.; Lu, Z.-H.; Bender, T. P. Boron Subphthalocyanines as Triplet Harvesting Materials within Organic Photovoltaics. *J. Phys. Chem. Lett.* **2015**, *6*, 3121−3125.
(183) Wilcox, D. E.; Lee, M. H.; Sykes, M. E.; Niedringhaus, A.; Geva, E.; Dunietz, B. D.; Shtein, M.; Ogilvie, J. P. Ultrafast Charge-Transfer Dynamics at the Boron Subphthalocyanine Chloride/C_{60} Heterojunction: Comparison between Experiment and Theory. *J. Phys. Chem. Lett.* **2015**, *6*, 569−575.
(184) Sánchez-Molina, I.; Claessens, C. G.; Grimm, B.; Guldi, D. M.; Torres, T. Trapping Fullerenes with Jellyfish-Like Subphthalocyanines. *Chem. Sci.* **2013**, *4*, 1338−1344.
(185) Iglesias, R. S.; Claessens, C. G.; Torres, T.; Rahman, G. M. A.; Guldi, D. M. Synthesis and Photophysical Characterization of a Subphthalocyanine Fused Dimer−C_{60} Dyad. *Chem. Commun.* **2005**, 2113−2115.
(186) Shimizu, S.; Nakano, S.; Hosoya, T.; Kobayashi, N. Pyrene-Fused Subphthalocyanine. *Chem. Commun.* **2011**, *47*, 316−318.
(187) Camerel, F.; Ulrich, G.; Retailleau, P.; Ziessel, R. Ethynyl−Boron Subphthalocyanines Displaying Efficient Cascade Energy Transfer and Large Stokes Shifts. *Angew. Chem., Int. Ed.* **2008**, *47*, 8876−8880.
(188) Yanai, T.; Tew, D.; Handy, N. A New Hybrid Exchange−Correlation Functional Using the Coulomb-Attenuating Method (CAM-B3LYP). *Chem. Phys. Lett.* **2004**, *393*, 51−57.
(189) Tawada, Y.; Tsuneda, T.; Yanagisawa, S.; Yanai, T.; Hirao, K. A Long-Range-Corrected Time-Dependent Density Functional Theory. *J. Chem. Phys.* **2004**, *120*, 8425.
(190) Vydrov, O. A.; Scuseria, G. E. Assessment of a Long-Range Corrected Hybrid Functional. *J. Chem. Phys.* **2006**, *125*, No. 234109.
(191) Vydrov, O. A.; Heyd, J.; Krukau, A.; Scuseria, G. E. Importance of Short-Range Versus Long-Range Hartree-Fock Exchange for the Performance of Hybrid Density Functionals. *J. Chem. Phys.* **2006**, *125*, No. 074106.
(192) Vydrov, O. A.; Scuseria, G. E.; Perdew, J. P. Tests of Functionals for Systems with Fractional Electron Number. *J. Chem. Phys.* **2007**, *126*, No. 154109.
(193) Grimme, S. Semiempirical GGA-Type Density Functional Constructed with a Long-Range Dispersion Correction. *J. Comput. Chem.* **2006**, *27*, 1787−1799.
(194) Chai, J.-D.; Head-Gordon, M. Long-Range Corrected Hybrid Density Functionals with Damped Atom−Atom Dispersion Corrections. *Phys. Chem. Chem. Phys.* **2008**, *10*, 6615−6620.
(195) Grimme, S.; Antony, J.; Ehrlich, S.; Krieg, S. A Consistent and Accurate ab initio Parametrization of Density Functional Dispersion Correction (DFT-D) for the 94 Elements H-Pu. *J. Chem. Phys.* **2010**, *132*, No. 154104.
(196) Hu, J.-Y.; Era, M.; Elsegood, M. R. J.; Yamato, T. Synthesis and Photophysical Properties of Pyrene-Based Light-Emitting Monomers: Highly Pure-Blue-Fluorescent, Cruciform-Shaped Architectures. *Eur. J. Org. Chem.* **2010**, 72−79.
(197) Salini, P. S.; Rajagopal, S. K.; Hariharan, M. Haloacetylation-Driven Transformation of Sandwich Herringbone to Lamellar/Columnar Packing in Pyrene. *Cryst. Growth Des.* **2016**, *16*, 5822−5830.
(198) Kobayashi, M.; Hayakawa, N.; Matsuo, T.; Li, B.; Fukunaga, T.; Hashizume, D.; Fueno, H.; Tanaka, K.; Tamao, K. (Z)-1,2-Di(1-Pyrenyl)Disilene: Synthesis, Structure, and Intramolecular Charge-Transfer Emission. *J. Am. Chem. Soc.* **2016**, *138*, 758−761.
(199) Chou, T.-C.; Hwa, C.-L.; Lin, J.-J.; Liao, K.-C.; Tseng, J.-C. Bicyclo[2.2.2]Octene-Based "Crab-like" Molecules: Synthesis, Complexation, Luminescence Properties, and Solid-State Structures. *J. Org. Chem.* **2005**, *70*, 9717−9726.
(200) Killoran, J.; Allen, L.; Gallagher, J. F.; Gallagher, W. M.; O'Shea, D. F. Synthesis of BF_2 Chelates of Tetraarylazadipyrromethenes and Evidence for their Photodynamic Therapeutic Behavior. *Chem. Commun.* **2002**, 1862−1863.
(201) Bublitz, D. E.; Rinehart, K. L. The Synthesis of Substituted Ferrocenes and other π-Cyclopentadienyl-Transition Metal Compounds. *Org. React.* **1969**, *17*, 1−154.
(202) D'Aléo, A.; Karapetyan, A.; Heresanu, V.; Giorgi, M.; Fages, F. Tuning Solid-State Emission Properties of Pyrene-Containing Chalcone Derivatives. *Tetrahedron* **2015**, *71*, 2255−2259.
(203) D'Aléo, A.; Gachet, D.; Heresanu, V.; Giorgi, M.; Fages, F. Efficient NIR-Light Emission from Solid-State Complexes of Boron Difluoride with 2′-Hydroxychalcone Derivatives. *Chem. − Eur. J.* **2012**, *18*, 12764−12772.

DOI: 10.1021/acs.jpcc.8b09504
J. Phys. Chem. C 2018, 122, 27893−27916

(204) Feng, Q.; Wang, M.; Dong, B.; Xu, C.; Zhao, J.; Zhang, H. Tuning Solid-State Fluorescence of Pyrene Derivatives via a Cocrystal Strategy. *CrystEngComm* **2013**, *15*, 3623−3629.
(205) Xiao, Z.; Shi, Y.; Sun, R.; Ge, J.; Li, Z.; Fang, Y.; Wu, X.; Yang, J.; Zhao, M.; Song, Y. Ultrafast Broadband Optical Limiting in Simple Pyrene-Based Molecules with High Transmittance from Visible to Infrared Regions. *J. Mater. Chem. C* **2016**, *4*, 4647−4653.
(206) Hou, P.-X.; Liu, C.; Cheng, H.-M. Purification of Carbon Nanotubes. *Carbon* **2008**, *46*, 2003−2025.
(207) Wells, N. P.; Boudouris, B. W.; Hillmyer, M. A.; Blank, D. A. Intramolecular Exciton Relaxation and Migration Dynamics in Poly(3-hexylthiophene). Intramolecular exciton Relaxation and Migration Dynamics in Poly(3-Hexylthiophene). *J. Phys. Chem. C* **2007**, *111*, 15404−15414.
(208) Becke, A. D. Density-Functional Thermochemistry. III. The Role of Exact Exchange. *J. Chem. Phys.* **1993**, *98*, 5648−5652.
(209) Lee, C.; Yang, W.; Parr, R. G. Development of the Colle-Salvetti Correlation-Energy Formula into a Functional of the Electron Density. *Phys. Rev. B* **1988**, *37*, 785−789.
(210) Tamada, M.; Iino, T.; Wang, Y.; Ide, M.; Saeki, A.; Furuta, H.; Kobayashi, N.; Shimizu, S. Facile Synthesis of Dimeric Aza-BODIPY Analogues from Electron-Deficient Bislactams and their Intriguing Optical and Electrochemical Properties. *Tetrahedron Lett.* **2017**, *58*, 3151−3154.
(211) Liu, Y.; Duan, J.; Qi, F.; Tian, D.; Wang, X.; Liu, Z.; Huang, W. Optical Properties and Mechanofluorochromism of New BODIPY Dyes Based on the Pyridine−Pyrimidine Hybrid Structure. *Dalton Trans.* **2017**, *46*, 10332−10338.
(212) Epelde-Elezcano, N.; Palao, E.; Manzano, H.; Prieto-Castaneda, A.; Agarrabeitia, A. R.; Tabero, A.; Villanueva, A.; de la Moya, S.; Lopez-Arbeloa, I.; Martinez-Martinez, V.; Ortiz, M. J. Rational Design of Advanced Photosensitizers Based on Orthogonal BODIPY Dimers to Finely Modulate Singlet Oxygen Generation. *Chem. − Eur. J.* **2017**, *23*, 4837−4848.
(213) Zhao, N.; Xuan, S.; Fronczek, F. R.; Smith, K. M.; Vicente, M. G. H. Enhanced Hypsochromic Shifts, Quantum Yield, and $\pi-\pi$ Interactions in a meso, β-Heteroaryl-Fused BODIPY. *J. Org. Chem.* **2017**, *82*, 3880−3885.
(214) Christianson, A. M.; Gabbai, F. P. Anion Sensing with a Lewis Acidic BODIPY-Antimony(V) Derivative. *Chem. Commun.* **2017**, *53*, 2471−2474.
(215) Goetsch, W. R.; Solntsev, P. V.; Van Stappen, C.; Purchel, A. A.; Dudkin, S. V.; Nemykin, V. N. Electron-Transfer Processes in 3,4-Diferrocenylpyrroles: Insight into a Missing Piece of the Poly-ferrocenyl-Containing Pyrroles Family. *Organometallics* **2014**, *33*, 145−157.
(216) Scalmani, G.; Frisch, M. J.; Mennucci, B.; Tomasi, J.; Cammi, R.; Barone, V. Geometries and Properties of Excited States in the Gas Phase and in Solution: Theory and Application of a Time-Dependent Density Functional Theory Polarizable Continuum Model. *J. Chem. Phys.* **2006**, *124*, No. 094107.
(217) Wachters, A. J. H. Gaussian Basis Set for Molecular Wavefunctions Containing Third-Row Atoms. *J. Chem. Phys.* **1970**, *52*, 1033−1036.
(218) McLean, A. D.; Chandler, G. S. Contracted Gaussian Basis Sets for Molecular Calculations. I. Second Row Atoms, Z = 11−18. *J. Chem. Phys.* **1980**, *72*, 5639−5648.
(219) Frisch, M. J.; Trucks, G. W.; Schlegel, H. B.; Scuseria, G. E. *Gaussian 09*, revision D.1; Gaussian, Inc.: Wallingford, CT, 2009. For full citation, see Supporting Information.
(220) Tenderholt, A. L. *QMForge*, version 2.1; Stanford University: Stanford, CA, http://qmforge.sourceforge.net/.
(221) Altomare, A.; Cascarano, G.; Giacovazzo, C.; Guagliardi, A.; Burla, M. C.; Polidori, G.; Camalli, M. SIRPOW 92 a Program for Automatic Solution of Crystal Structures by Direct Methods Optimized for Powder Data. *J. Appl. Crystallogr.* **1994**, *27*, 435.
(222) Bellizzi, M.; Foss, P. C. D.; Pelto, R.; Crundwell, G.; Brückner, C.; Updegraff, J. B., III; Zeller, M.; Hunter, A. D. Crystal Structure of 5,10,15,20-Tetrakis(5′-Methylthien-2′-yl)Porphyrin, $C_{40}H_{30}N_4S_4$. *Z. Kristallogr.* **2004**, *219*, 129−131.
(223) Wagner, P.; Officer, D. L.; Kubicki, M. 2,5-Bis(2-Cyano-2-Thienylvinyl)Thiophene. *Acta Crystallogr., Sect. E: Struct. Rep. Online* **2006**, *62*, o5745−o5747.
(224) Betteridge, P. W.; Carruthers, J. R.; Cooper, R. I.; Prout, K.; Watkin, D. J. CRYSTALS Version 12: Software for Guided Crystal Structure Analysis. *J. Appl. Crystallogr.* **2003**, *36*, 1487.
(225) *APEX3*, v2016.1-0; Bruker-AXS: Madison, Wisconsin, 2016.
(226) Sheldrick, G. M. Crystal Structure Refinement with SHELXL. *Acta Crystallogr., Sect. A: Found. Adv.* **2008**, *64*, 112−122.
(227) Spek, A. L. Structure Validation in Chemical Crystallography. *Acta Crystallogr., Sect. D: Biol. Crystallogr.* **2009**, *65*, 148−155.

DOI: 10.1021/acs.jpcc.8b09504
J. Phys. Chem. C 2018, 122, 27893−27916